

Gas pile-up, gap overflow, and Type 1.5 migration in circumbinary disks: general theory

Bence Kocsis^{1,3*}, Zoltán Haiman^{2†} and Abraham Loeb^{1‡}

¹*Harvard-Smithsonian Center for Astrophysics, 60 Garden St., Cambridge, MA 02138, USA*

²*Department of Astronomy, Columbia University, 550 West 120th Street, New York, NY 10027*

³*Einstein Fellow*

5 November 2018

ABSTRACT

Many astrophysical binaries, from planets to black holes, exert strong torques on their circumbinary accretion disks, and are expected to significantly modify the disk structure. Despite the several decade long history of the subject, the joint evolution of the binary + disk system has not been modeled with self-consistent assumptions for arbitrary mass ratios and accretion rates. Here we solve the coupled binary-disk evolution equations analytically in the strongly perturbed limit, treating the azimuthally-averaged angular momentum exchange between the disk and the binary and the modifications to the density, scale-height, and viscosity self-consistently, including viscous and tidal heating, diffusion limited cooling, radiation pressure, and the orbital decay of the binary. We find a solution with a central cavity and a migration rate similar to those previously obtained for Type-II migration, applicable for large masses and binary separations, and near-equal mass ratios. However, we identify a distinct new regime, applicable at smaller separations and masses, and mass ratio in the range $10^{-3} \lesssim q \lesssim 0.1$. For these systems, gas piles up outside the binary’s orbit, but rather than creating a cavity, it continuously overflows as in a porous dam. The disk profile is intermediate between a weakly perturbed disk (producing Type-I migration) and a disk with a gap (with Type-II migration). However, the migration rate of the secondary is typically slower than both Type-I and Type-II rates. We term this new regime “Type-1.5” migration.

Key words: accretion, accretion discs – black hole physics – gravitational waves – galaxies: active

1 INTRODUCTION

Understanding the co-evolution of binaries and accretion disks is fundamental in several fields of astrophysics, including planet formation and migration (Goldreich & Tremaine 1980; Ward 1997), patterns in planetary rings (Goldreich & Tremaine 1982), stellar binaries, compact object, and binaries involving supermassive black holes (SMBHs).

Despite the long history of the subject, there are no self-consistent analytical models for the co-evolution of binaries and accretion disks, incorporating the fundamental physical effects over the long timescales on which the binary separation evolves. The standard α -model of radiatively efficient turbulent thin accretion disks (Shakura & Sunyaev

1973) relates the effective kinematic viscosity of the disk to the pressure $\nu \propto \alpha p$. The viscous evolution of the disk, however, is often modeled without considering the pressure dependence of the viscosity (Lynden-Bell & Pringle 1974). Similarly, models of the gravitational interaction between the disk, which describe the launching of spiral density waves in the disk that remove angular momentum from the binary, also do not account for the tidal heating of the disk and the corresponding feedback on the torque cutoff phenomenon (Goldreich & Tremaine 1980).

The evolution of the circumbinary disk is sensitive to the above mentioned assumptions, especially when the mass of the secondary is large, and can strongly perturb the disk. For a massive secondary, the tidal torque clears a gap in the disk, and the viscous radial inflow of the gas pushes the object inward on the viscous timescale (Type-II migration). If the secondary mass, m_s is larger than the local disk mass, $m_d = 4\pi r^2 \Sigma$, where Σ is the surface density, then the migration slows down, as the spiral density waves cannot

* E-mail: bkocsis@cfa.harvard.edu

† E-mail: zoltan@astro.columbia.edu

‡ E-mail: aloeb@cfa.harvard.edu

remove angular momentum away from the binary at a rate on which the gas flows in. This leads to the pile-up of gas outside the secondary’s orbit, in which the gas density increases by up to a factor $B^{-3/8}$, where $B = m_{d0}/m_s < 1$ and m_{d0} is the unperturbed local disk mass (Syer & Clarke 1995). Once this steady-state level is reached, the viscous gas inflow velocity matches the inward migration of the object (secondary dominated Type-II migration).

In this paper, we focus on such systems, with $m_s > m_{d0}$, and point out that the Syer & Clarke (1995) steady-state level of gas pile-up cannot be reached for sufficiently large secondary masses $m_s \gg m_{d0}$, where $B \ll 1$. The enhanced viscous dissipation rate ($D_\nu \propto B^{-5/8}$) can increase the disk temperature such that it becomes radiation pressure dominated. The enhanced pressure makes the disk puff up ($H \propto B^{-5/8}$), and reduces the relative gap size. Once the gas approaches within a distance less than the scale-height from the secondary, the torque that the disk exerts on the binary has a cutoff (Goldreich & Tremaine 1980; Artymowicz 1993b,a; Goodman & Rafikov 2001) which limits the migration rate of the secondary. Once the gas enters the Hill radius, it can furthermore flow across the secondary’s orbit along horseshoe orbits or accrete onto the secondary. We derive an analytical quasi-steady-state model for the co-evolution of the disk and the orbital migration of the secondary, in which we combine a Shakura & Sunyaev (1973) disk with the theory of the binary-disk interaction by Goldreich & Tremaine (1980) self-consistently. In particular, we adopt the viscosity prescription of standard thin accretion disks proportional to pressure,¹ calculate the sound speed and vertical balance including both gas and radiation pressure (p_{gas} and p_{rad}), adopt the simple analytical approximation to the angular momentum exchange between the binary and the disk of Armitage & Natarajan (2002), consider the standard viscous and tidal heating of the disk (Lodato et al. 2009), and self-consistently account for the feedback on the pressure, viscosity, scale-height, and the torque cutoff near the secondary’s orbit. We generalize the steady-state model of Hourigan & Ward (1984), Ward & Hourigan (1989), and Liu & Shapiro (2010) by self-consistently including variations in the viscosity and pressure caused by the pile-up. We derive azimuthally averaged steady-state analytical disk models which recover the Goodman & Tan (2004) solution for arbitrary $\beta = p_{\text{gas}}/(p_{\text{gas}} + p_{\text{rad}})$ in the limit that the secondary mass m_s approaches zero, but the disk structure is significantly modified by the secondary over multiple accretion timescales for larger m_s .

The disk structure in this overflowing state with a pile-up is intermediate between the weakly perturbed case without a secondary and the case with a gap. Not surprisingly, the migration rate in such an intermediate state, which we label Type-1.5, is significantly different from the corresponding limiting cases of Type-I migration and the secondary-dominated Type-II migration. The transition between Type-I and Type-II migration as a function of the

¹ Here $\nu \propto p_{\text{gas}}$ and $\nu \propto (p_{\text{gas}} + p_{\text{rad}})$ are respectively known as α and β -models. We formulate our problem for a general α or β -disk in Sec. 2, but then derive the analytical results for the special case of a β disk viscosity.

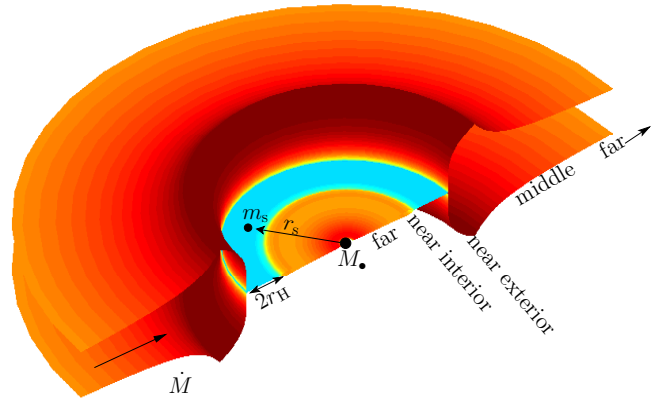


Figure 1. Gas pile-up and overflow in a circumbinary accretion disk with component masses M_\bullet and m_s , binary separation r_s , and accretion rate \dot{M} . We distinguish five distinct radial zones: an inner and an outer far zone where the effects of the secondary are negligible, an interior and an exterior near zone where the tidal effects are significant, and an extended middle zone with a significant gas pile-up (see § 4).

secondary mass was previously typically investigated by considering only the change in the surface density due to gap formation, but without investigating the feedback from the changes in viscosity and pressure (Hourigan & Ward 1984; Ward & Hourigan 1989; Korycansky & Papaloizou 1996; Ward 1997; Bate et al. 2003; Crida & Morbidelli 2007). However, simulations show that migration is sensitive to temperature variations and radiation pressure (D’Angelo et al. 2003; Paardekooper & Mellema 2006, 2008; Kley & Crida 2008). We derive the Type-1.5 migration rate for the self-consistent radial profile including these effects when the pile-up is significant in an overflowing steady-state disk. As the secondary migrates inwards across the increasingly hotter inner regions of the disk, the gap opening conditions and the migration rate change even if one neglects the feedback on viscosity and temperature due to gas pile-up (Haiman et al. 2009; Kocsis et al. 2011), but here we show that the changes are significant over a much wider range of masses and radii in the self-consistent model. We discuss migration and gap opening for SMBH binaries in more detail in Kocsis et al. (2012), hereafter Paper II.

The remainder of the paper is organized as follows. In § 2, we lay out the basic equations governing the hydrodynamical and thermal evolution of the disk, as well as the migration of the secondary. We solve the equations numerically in § 3. We then derive an analytical solution in § 4. We summarize the results, and discuss how they depend on the most important physical parameters, in § 5. We offer our conclusions in § 6. A more detailed discussion and the implications for SMBH binary systems is presented in Paper II.

We use geometrical units $G = c = 1$, and suppress factors of G/c^2 and G/c^3 to convert between mass, length, and time units. Our basic notation for the disk and secondary parameters are depicted in Figure 1.

2 THERMO-HYDRODYNAMICAL INTERACTION BETWEEN A DISK AND A SECONDARY

We examine the evolution of the secondary and an azimuthally and vertically averaged Shakura-Sunyaev disk (i.e. axisymmetric one-zone disk) in local thermal equilibrium. Here we review the basic equations. First, we write down the continuity and angular momentum transport equations including the viscous torque and the gravitational tidal torque of the secondary. The back-reaction of the tidal torque changes the angular momentum of the secondary. The viscous and tidal torques depend on the disk surface density, viscosity, and pressure gradient (or scale-height). We derive the vertically averaged disk structure assuming that: (i) the local viscous plus tidal heating equals the radiative cooling with photon diffusion limited vertical radiative flux (i.e. negligible radial heat transport); (ii) the viscosity is proportional to either gas+radiation pressure (α -disk) or just the gas pressure (β -disk), and (iii) gas plus radiation pressure supports the disk against the vertical gravity. This yields a closed set of nonlinear partial differential equations for the disk and the location of the secondary in 1+1 dimensions. We present solutions in subsequent sections below.

2.1 Angular momentum transport

We denote the masses of the primary and the secondary objects by M_\bullet and m_s , the surface density of the disk by Σ (assuming axisymmetry), and the radial bulk velocity of the disk by v_r , which is negative if gas accretes toward $r = 0$. The continuity and angular momentum equations for the disk are²

$$0 = 2\pi r \partial_t \Sigma + \partial_r (2\pi r \Sigma v_r), \quad (1)$$

$$\partial_r T = 2\pi r \partial_t (\Sigma r^2 \Omega) + \partial_r (2\pi r v_r \Sigma r^2 \Omega), \quad (2)$$

where the total torque $T = -T_\nu + T_d$ is due to viscosity and the gravity of the secondary, given by

$$T_\nu = -2\pi r^3 (\partial_r \Omega) \nu \Sigma \simeq 3\pi r^2 \Omega \nu \Sigma, \quad (3)$$

$$\partial_r T_d = 2\pi r \Lambda \Sigma. \quad (4)$$

Here Λ is the torque per unit mass in the disk, approximately given by

$$\Lambda \approx \begin{cases} -\frac{1}{2} f q^2 r^2 \Omega^2 r_s^4 / \Delta^4 & \text{if } r < r_s, \\ +\frac{1}{2} f q^2 r^2 \Omega^2 r_s^4 / \Delta^4 & \text{if } r > r_s, \end{cases} \quad (5)$$

where

$$\Delta \equiv \max(|r - r_s|, H) \quad (6)$$

$q \equiv m_s / M_\bullet$, $H \ll r$ is the scale-height of the disk, and f is a constant calibrated with simulations. This approximate formula for Λ , introduced by Armitage & Natarajan (2002), accounts for the net contribution of all Lindblad resonances as well as the torque cutoff within $r_s \pm$

² In our notation, $\partial_r \Sigma \equiv \partial \Sigma / \partial r$ and $\partial_t \Sigma \equiv \partial \Sigma / \partial t \equiv \dot{\Sigma}$. T refers to torque, T_ν and T_d are viscous and tidal torques as in Chang et al. (2010); Liu & Shapiro (2010). The angular momentum flux is $F_j \equiv T$. Central and surface temperatures are labelled with T_c and T_s .

H (Goldreich & Tremaine 1980; Ward 1997), and guarantees that the torque vanishes at $r \gg r_s$. Here $f = (32/81\pi)[2K_0(2/3) + K_1(2/3)]^2 = 0.80$ outside the torque cutoff in Goldreich & Tremaine (1980), $f = 0.23 \times (3/2\pi) = 0.11$ in Lin & Papaloizou (1986), and $f = 10^{-2}$ calibrated to match the gap opening conditions in Armitage & Natarajan (2002).³ We adopt a conservative value $f_{-2} \equiv f/10^{-2} \sim 1$ in our numerical calculations, but keep the f_{-2} terms general in all of our analytical formulas. Note that practically Eq. (6) assumes that the tidal torque density ‘‘saturates’’ instead of having a true cutoff near the secondary as long as the gas density is non-vanishing there (Artymowicz 1993b), which accounts for the effects of shocks near the secondary (Goodman & Rafikov 2001; Dong et al. 2011; Duffell & MacFadyen 2012).^{4 5} However, this prescription might be inaccurate for a high-mass secondary forming a gap in the disk, where the tidal torques are due to spiral streams passing near the secondary on horse-shoe orbits (MacFadyen & Milosavljević 2008; Shi et al. 2012; Roedig et al. 2012; Baruteau et al. 2012; Petrovich & Rafikov 2012). We do not consider the torques inside the Hill radius, $|r - r_s| < r_H \equiv (q/3)^{1/3} r_s$, assuming that gas reaching this region flows in across the secondary’s orbit. Outside this region, we use Eq. (4), assume that gravity is dominated by M_\bullet , and the orbital velocity is nearly Keplerian, $\Omega \simeq M_\bullet \bar{r}^{-3/2}$, where $\bar{r} = r/M_\bullet$.

After some algebra (Frank et al. 2002), Eqs. (1–2) simplify to

$$\dot{\Sigma} = -\frac{1}{2\pi r} \partial_r \left[\frac{\partial_r T}{\partial_r (r^2 \Omega)} \right], \quad v_r = \frac{\partial_r T}{2\pi r \Sigma \partial_r (r^2 \Omega)}. \quad (7)$$

The total mass flux across a ring of radius r is defined as

$$\dot{M}(r, t) \equiv -2\pi r \Sigma v_r = -\frac{\partial_r T}{\partial_r (r^2 \Omega)}. \quad (8)$$

Eq. (7) along with the definition of the total torque T in Eqs. (3–5) describes the evolution of the axisymmetric disk surface density and radial velocity as a function of radius and time.

The evolution of the secondary’s orbital radius, r_s , is driven by the tidal torques of the gas and gravitational wave (GW) losses. The angular momentum of the secondary is $L_s = m_s r_s^2 \Omega_s$ so that

$$\dot{L}_s = \frac{1}{2} m_s r_s \Omega_s v_{sr} = -\int_0^\infty \partial_r T_d dr - T_{GW}, \quad (9)$$

³ Liu & Shapiro (2010) used Eq. (5) with $f = 10^{-2}$. Chang et al. (2010) adopted a torque model, extrapolating Eq. (18) of Goldreich & Tremaine (1980) (with a modified constant prefactor of $f = 0.1 \times (4/9\pi) \sim 10^{-2}$), such that their torque density approaches a constant at $r \gg r_s$. The linear perturbative analysis of Goldreich & Tremaine (1980) is not applicable if $q \gtrsim \alpha^2$ or $q \gtrsim (H/r)^3$ (Meyer-Vernet & Sicardy 1987; Ward 1997; Korycansky & Papaloizou 1996).

⁴ Recent simulations (Dong et al. 2011; Rafikov & Petrovich 2012; Duffell & MacFadyen 2012) have shown that the original Goldreich & Tremaine (1980) torque density is correct close to the secondary, but the actual torque decreases in amplitude and changes sign outside of $r_s + 3H$. However the relative contribution of these outer regions to the total torque is negligible.

⁵ We do not account for relativistic corrections to the tidal torque which are expected to be small at the separations in the gas-driven regime $r_s > 100M_\bullet$ (Hirata 2011a,b).

where $-T_d$ is the recoil due to the torque exerted on the disk, Eq. (4), and with $\bar{r}_s \equiv r_s/M_\bullet$, the torque from the GWs is given by

$$T_{\text{GW}} = \frac{32}{5} \frac{m_s^2}{M_\bullet} \bar{r}_s^{-7/2}. \quad (10)$$

Given $\nu(r, t)$ and $H(r, t)$, Eqs. (7) and (9) provide three equations for the three unknowns: $\Sigma(r, t)$, $v_r(r, t)$, and $v_{\text{sr}}(t)$.

We examine steady-state solutions to these equations where $\dot{\Sigma} = 0$ and $d\dot{M}/dr = 0$ so that $\dot{M}(r, t) \equiv \dot{M}$ is a constant.⁶ Note that in general the disk need not be in steady-state. However, in many cases the inflow rate of gas may be much faster than the radial migration speed of the secondary $|v_{\text{sr}}| \ll |v_r|$. If this is satisfied in a wide range of radii up to the outer edge of the disk, then, the secondary is effectively stationary in the azimuthally averaged picture, and the radial profile of the disk might be expected to relax to a steady-state, independent of the initial condition of the disk. We propose that the secondary then migrates slowly through a sequence of quasi-steady-state configurations of the disk with a fixed $\dot{M}(r, t) = \text{const}$. Then, Eq. (8) becomes

$$\partial_r T_\nu - \partial_r T_d = \dot{M} \partial_r (r^2 \Omega). \quad (11)$$

This is a first-order ordinary differential equation for $T_\nu(r)$, once $\partial_r T_d(r)$ is specified for a specific disk model.

2.2 Boundary conditions

We distinguish two types of inner boundary conditions corresponding to whether or not the perturbation is strong enough to lead to a truncated disk with a wide hollow circular cavity. Here, “wide” means wider than the Hill radius (see below).

I. If $\Sigma(r) \neq 0$ all the way to the innermost stable circular orbit r_{ISCO} of M_\bullet (i.e. the disk does not have a cavity), we require a zero-torque boundary condition (Novikov & Thorne 1973; Penna et al. 2010; Tanaka 2011; Zhu et al. 2012),

$$T_\nu(r_{\text{ISCO}}) = 0. \quad (12)$$

Starting with this boundary condition, we obtain, among other properties of the steady-state disk, the gas velocity profile $v_r(r)$. As stated above, if this inflow velocity is much faster than the migration velocity of the secondary over a large range of radii, then one might expect that the disk approaches this steady-state configuration, independent of the initial condition. In the opposite case, the steady-state assumption may be violated by the time-dependent migration of the secondary. As we will show, the steady-state solution with a fixed \dot{M} requires a large build-up of gas outside the secondary for the viscosity to overcome the tidal barrier of the secondary. We refer to these solutions, in which the disk is not truncated outside the secondary as “overflowing”.

II. If the tidal torques dominate over the viscous torques near the secondary, gas is expelled from the region near the secondary and a wide gap forms. Assuming that the characteristic radius r_g , where the tidal torque is exerted on the disk near the edge of the gap, tracks the inward migration

⁶ As stated above, we neglect the accretion onto the secondary for simplicity (however, see Lubow et al. 1999).

of the secondary with $r_g = \lambda r_s$ where $1 < \lambda \lesssim 3$ is a constant, we require that the gas velocity at that radius satisfy (Syer & Clarke 1995; Ivanov et al. 1999)

$$v_r(\lambda r_s) = \lambda v_{\text{sr}}. \quad (13)$$

Note that λ is not specified by hand ab-initio; it is found by assuming steady-state in our solutions below. This condition can be understood intuitively, since the secondary cannot “run away” and leave the outer disk behind (if it did, it would cease to be able to torque the disk and would have to slow down). Likewise, the gap edge cannot get closer to the secondary (if it did, gas would pile-up and the gap would eventually close). Although the disk is not in steady-state near its boundary, we assume $\dot{M}(r) \approx \dot{M}$ at $r > r_g$ (see discussion in § 4.1.4 below).

Based on Eq. (8) and (9), Eq. (13) is equivalent to

$$\int_0^\infty \partial_r T_d dr = \frac{m_s r_s^2 \Omega_s \dot{M}}{4\pi r_g^2 \Sigma(r_g)} - T_{\text{GW}}. \quad (14)$$

Note that here and throughout the paper by “gap” we refer to situations where the gas density becomes effectively zero outside the secondary, such that the inflow of gas from the outside pushes the secondary inward according to (13). In these cases, we assume that inflow across the orbit is insignificant, and in particular, we neglect torques from the gas interior to the orbit. In our calculations, a gap is effectively a hollow circular cavity in the disk, which is supported by the tidal torques of the secondary. However we emphasize that we do not rule out the presence of a local density decrement, resembling an annular gap, with a significant mass flux across the gap.

In practice, we attempt to find a solution with either of the above two boundary conditions, and then check whether the solution is self-consistent. By construction, only one of the two boundary conditions will lead to a self-consistent solution as confirmed below.

2.3 Physical conditions in the disk

Next we derive $H(r)$ and $\nu(r)$ which appear in the tidal and viscous torques in Eqs. (3–5).

2.3.1 Vertical balance

Let us first derive the scale-height, H . If the vertical gravity is dominated by M_\bullet , (i.e. $|r - r_s| > r_H$), then in vertical hydrostatic equilibrium $H = c_s/\Omega$ where $c_s = \sqrt{p/\rho}$ is the local midplane sound speed and $p = p_{\text{gas}} + p_{\text{rad}}$ is the pressure due to the gas and radiation⁷, $p_{\text{gas}} = \rho k T_c / (\mu m_p)$, $p_{\text{rad}} = \frac{1}{3} a T_c^4$, where T_c is the central temperature, $a = 4\sigma/c$ is the radiation constant, σ is the Stefan-Boltzmann constant, m_p is the proton mass, and $\mu = 0.615$ is the mean particle mass in units of m_p . Since $\rho = \Sigma/(2H)$, $c_s^2 = 2Hp/\Sigma = 2c_s p/(\Sigma\Omega)$ so that $c_s = 2p/(\Sigma\Omega)$. The pressure can be expressed as

⁷ Note that the gas is *not* degenerate and is *not* isentropic, therefore the assumption of $p \propto \rho^{5/3}$ or $\rho^{4/3}$ made in most numerical simulations of accretion disks is inappropriate. In fact, $p \propto T^4 \propto \dot{M}^4 \rho^6$ for a radiation-pressure dominated standard Shakura-Sunyaev disk with no secondary.

$p = p_{\text{rad}}/(1 - \beta)$, where $\beta = p_{\text{gas}}/p$. If photons are transported to the surface by diffusion then the mean radiation flux is

$$F = \sigma T_s^4 = \frac{4}{3} \frac{\sigma T_c^4}{\tau} = \frac{8}{3} \frac{\sigma T_c^4}{\kappa \Sigma} \quad (15)$$

Here T_s is the surface temperature, $\tau = \kappa \Sigma / 2$ is the optical depth from the midplane to the surface, where $\kappa = 0.35 \text{ cm}^2/\text{g}$ is the opacity assumed to be dominated by electron-scattering. We do not investigate changes caused by free-free opacity at large radii for simplicity, and neglect deviations from blackbody radiation (see e.g. Tanaka & Menou 2010 for more a detailed model). Thus, $p_{\text{rad}} = \frac{1}{2} \kappa \Sigma F / c$, so that $c_s = \kappa c^{-1} F \Omega^{-1} (1 - \beta)^{-1}$, and we have

$$H = \frac{c_s}{\Omega} = \frac{\kappa}{c \Omega^2} \frac{F}{1 - \beta} \quad (16)$$

Note that Eq. (16) is valid in general for radiation flux limited, geometrically thin disks, independent of the source of dissipation and viscosity.⁸

2.3.2 Viscosity

In the standard Shakura-Sunyaev α and β -disk models, the viscous stress tensor, $t_{ij} = \rho \nu \nabla_i v_j$ satisfies $t_{r\phi} = -\frac{3}{2} \alpha \beta^b p$, where $b = 0$ or 1 , respectively, and α is a constant parameter (Shakura & Sunyaev 1973; Sakimoto & Coroniti 1981), implying that

$$\nu = \alpha c_s H \beta^b = \alpha \frac{\kappa^2}{c^2 \Omega^3} \frac{\beta^b F^2}{(1 - \beta)^2}. \quad (17)$$

In the second equality, we have substituted Eq. (16).

2.3.3 Local thermal equilibrium

We assume steady-state thermal equilibrium in which heat generated by viscosity and the dissipation of the spiral density wave escapes the optically thick disk in the vertical direction by photon diffusion. The vertical radiation flux is $F = D_\nu + D_d$. The viscous dissipation rate per disk face element is

$$D_\nu = \frac{(\partial_r \Omega) T_\nu}{4\pi r} = \frac{9}{8} \Omega^2 \nu \Sigma. \quad (18)$$

We assume that the density waves generated by the tidal torque are dissipated locally in the disk and turned into heat, yielding the rate D_d . This is expected to be an adequate approximation based on analytical arguments (Goldreich & Tremaine 1980, Eq. 97 therein) and numerical studies (Dong et al. 2011; Rafikov & Petrovich 2012; Duffell & MacFadyen 2012), especially in the regime where the disk is strongly perturbed.

⁸ One possible source of inconsistency is that convective vertical heat transport is conventionally neglected here. This may be significant for optically very thick, radiation pressure dominated disks (especially so-called β disks) with a large vertical temperature gradient (Blaes et al. 2011). The heat transport in this regime may be analogous to the convection zones of stars.

Following Goodman & Rafikov (2001) and Lodato et al. (2009)⁹,

$$D_d = \frac{(\Omega_s - \Omega) \partial_r T_d}{4\pi r} = \frac{1}{2} (\Omega_s - \Omega) \Lambda \Sigma. \quad (19)$$

The total vertical flux or total dissipation rate is

$$F = D_\nu + D_d = \frac{9}{8} \Omega^2 \nu \Sigma + \frac{1}{2} (\Omega_s - \Omega) \Lambda \Sigma. \quad (20)$$

Using the above equations we derive Σ and T_c for a given D_ν and F at each radius (see Appendix A).

2.3.4 Summary

Combining the previous expressions, we obtain

$$\Sigma = \frac{8 (\mu m_p / k)^{4/5} \sigma^{1/5} \beta^{(1-b)4/5} D_\nu^{4/5}}{3^{9/5} \alpha^{4/5} \kappa^{1/5} \Omega^{4/5} F^{1/5}}, \quad (21)$$

$$T_c = \frac{(\mu m_p / k)^{1/5} \kappa^{1/5} \beta^{(1-b)/5} F^{1/5} D_\nu^{1/5}}{3^{1/5} \alpha^{1/5} \sigma^{1/5} \Omega^{1/5}}, \quad (22)$$

where

$$\frac{\beta^{(1/2)+(b-1)/10}}{1 - \beta} = \frac{c [k / (\mu m_p)]^{2/5}}{(3 \alpha \sigma)^{1/10} \kappa^{9/10}} \Omega^{9/10} \frac{D_\nu^{1/10}}{F^{9/10}}. \quad (23)$$

All other disk parameters can be derived from these relations. For example, the scale-height H and the quantity $\nu \Sigma$ that determine the torque (Eq. 11) are given by Eqs. (16) and (18). In particular, the limiting cases for H are

$$H = \begin{cases} \kappa c^{-1} \Omega^{-2} F & \text{if } \beta \ll 1, \\ \sqrt{k / (\mu m_p)} \Omega T_c^{1/2} & \text{if } \beta \sim 1. \end{cases} \quad (24)$$

In the limit that the only source of heat is viscosity in a Keplerian disk, $F = D_\nu = (3/8\pi) \dot{M} \Omega^2$, we recover the solution of Goodman (2003) up to a constant of order unity.¹⁰

More generally, Eqs. (16), (21), and (23), along with the definition of D_ν and F in Eqs. (18) and (20), and the angular momentum flow equation (11) provide a closed set of equations for the stationary disk, valid throughout the gas and radiation-pressure dominated regions for α and β disks. The solution is self-consistent if for all r , the disk is thin ($H < r$), the radiation flux is sub-Eddington ($L \sim 2\pi r^2 F < 4\pi c G M_\bullet / \kappa$), the radial accretion velocity is subsonic ($v_r = \dot{M} / 2\pi r \Sigma < c_s = H \Omega$), radial heat transport is negligible, the self-gravity of the disk is negligible and the disk is stable against fragmentation ($Q = c_s \Omega / (\pi G \Sigma) \geq 1$), the disk is optically thick ($\tau = \kappa \Sigma / 2 \geq 1$), and the boundary conditions are satisfied (implying in particular that $v_{\text{sr}} \ll v_r$ across a wide range of radii for overflowing solutions, see § 2.2).¹¹

⁹ We add a factor of 2 that appears to be missing in Lodato et al. (2009); this enters because of the two disk faces.

¹⁰ We find a small difference in the density and temperature normalization constants, due to Goodman (2003) neglecting a $4/3$ prefactor in the vertical diffusion equation $F = \frac{4}{3} \sigma T_c^4 / \tau$.

¹¹ The model is furthermore self-consistent only outside the secondary's Hill sphere since the gravity of the secondary is accounted for as a perturbation to the primary's gravitational field, and the equations are linearized in the derivation of the torque formula. The tidal torque model is nevertheless often interpolated to within this region, as well (e.g. Goldreich & Tremaine 1980; Armitage & Natarajan 2002). Here we avoid this extrapolation by excising the region within the Hill radius from our domain, assuming that gas entering this region flows across the secondary orbit.

We verify that these conditions are indeed satisfied for the overflowing solutions below.

3 DISK STRUCTURE – NUMERICAL SOLUTIONS

First we generate numerical steady-state solutions for tidally and viscously heated disks assuming that the migration rate is much smaller than the radial accretion velocity in the disk. These numerical solutions are useful to verify the detailed analytical estimates presented in the following section.

We proceed along the following steps:

(i) Obtain the ratio of gas to total pressure, $\beta = \beta(r, D_\nu, F)$, by inverting Eq. (23). A unique solution is guaranteed by the intermediate value theorem, since the left hand side is a monotonic function of β , mapping $0 < \beta < 1$ to all positive real numbers, while the right hand side is positive and independent of β .

(ii) Substitute the solution for β in Eq. (16) and Eq. (21) to obtain $H(r, D_\nu, F)$ and $\Sigma(r, D_\nu, F)$.

(iii) Substitute β, H , and Σ in the definition of F , Eq. (20) to get an equation between F and D_ν for fixed r and r_s . Invert this relation to find $F(r, r_s, D_\nu)$. Similar to step (i), one can show that the solution exists and is unique.

(iv) Using Eqs. (18–19), obtain the function $\partial_r T_d = g_d(r, r_s, T_\nu)$.

(v) Substitute into Eq. (11), to obtain an expression $\partial_r T_\nu = g_\nu(r, r_s, T_\nu)$ for a fixed \dot{M} . Solve this differential equation for $T_\nu(r, r_s)$.

(vi) Substituting back into D_ν and F , Eqs. (18) and (20) and the formulas of step (ii), to get $\Sigma(r, r_s)$, $T_c(r, r_s)$, and $H(r, r_s)$.

The complexity is related to the nonlinearities in steps (i), (iii), and (v). Nevertheless, the solution exists and is unique in steps (i) and (iii). However, step (v) is a boundary value problem of a nonlinear first-order differential equation, which can have many solutions. We solve the differential equation numerically upstream from an initial value $T_\nu(r_{\text{ISCO}}) = 0$. Without the secondary, the solution is simply $T_{\nu 0}(r) = \dot{M}(r^2\Omega - r_{\text{ISCO}}^2\Omega_{\text{ISCO}})$, which leads to the Shakura-Sunyaev disk. If $q \ll 1$, then the secondary creates a small dip in $T_\nu(r)$ in its neighborhood, where the depth of the minimum increases with q . For larger q , $T_\nu(r)$ becomes very small positive approaching the secondary from downstream, and the surface density approaches zero. In this regime, tidal heating dominates over viscous heating, and $H > |r - r_s|$, implying that the pressure gradient shifts the torques out of resonance, and the torque is suppressed according to Eq. (5). Since the adopted torque model is valid only outside the secondary's Hill radius, we stop the calculation at $r_s - r_H$, and restart it at $r_i = r_s + r_H$ assuming that¹²

$$T_\nu(r_s - r_H) \approx T_\nu(r_i). \quad (25)$$

This has a similar effect to smoothing the torque interior

¹² The tidal torque is monotonically increasing and decreasing, interior and exterior the secondary, respectively. The solution is uniquely determined by the initial value $T_\nu(r_{\text{ISCO}})$ and $T_\nu(r, mi)$ in the two domains. However, r_i can be arbitrary as long as $r_0 > r_s$.

to the Hill radius as done previously in Lin & Papaloizou (1986), Syer & Clarke (1995), and Lodato et al. (2009).

The solution is approximately self-consistent if the migration rate is slower than the radial gas velocity outside the secondary. However, if this is not satisfied, a cavity opens and the disk becomes truncated. In this case, we seek a different solution in step (v), which satisfies the boundary condition in Eq. (13). This is possible by increasing r_i in Eq. (25) where $T_\nu(r_i) \approx 0$, until Eq. (37) is satisfied. Here r_i can be identified as the truncation radius at the inner edge of the disk. We distinguish the characteristic truncation or gap radius to reside at r_g where the tidal effect is exerted on the disk, more specifically the boundary where the tidal torque density becomes subdominant and use r_g in the boundary condition, Eq. (37).¹³ The surface density increases rapidly within $r_i < r \lesssim r_g$ has a maximum and decreases thereafter. We assume that the disk is truncated interior to r_i if a gap forms with $r_i > r_s + r_H$.

4 DISK STRUCTURE – ANALYTICAL SOLUTIONS

Here we derive an analytical solution to the nonlinear equations in § 2. Such solutions can be derived asymptotically far from the secondary or near the secondary, where either the tidal torque or the viscous torque dominates, or where the angular momentum flux is negligible. We therefore distinguish the corresponding far, middle, and near zones (see Figure 1). The *far zones* are well inside and well outside the secondary, where the effects of the secondary are negligible. The *middle zone* is the region outside the secondary where the tidal effects (i.e. torque and heating) are locally negligible compared to the viscous effects, but where the gas pile-up is significant and the disk profile is modified. The *near zones* are just inside and just outside the secondary's orbit, where the tidal effects of the secondary dominate over the viscous effects. We restrict the near zone to outside the Hill radius, where the adopted tidal torque formula is valid. In addition to providing a basic understanding of the disk structure, the approximate analytical solutions allow us to infer the migration rate of the secondary.

To keep track of the approximations and notations introduced for the various zones below, we provide Table 1 for convenience. Note that the far/middle/near zones divide the disk into five radial slices, and the asymptotic behavior further depends on whether the disk becomes truncated forming a wide gap (in the middle zone) and whether the torque is saturated by the condition on the radial distance from the secondary is $\delta r \equiv r - r_s < H$ (in the outer near-zone). Each row in the Table corresponds to one of these disk regimes, discussed in a corresponding subsection below,

¹³ In practice, we generate solutions for many different r_i . We seek the radius r_g at which the tidal torque cuts off in the numerical solution: $T_d(r_g) = 0.1 T_d(r_{\text{peak}})$ where $r_g > r_{\text{peak}}$ and r_{peak} is where $T_d(r)$ attains its maximum. We use this value as the gas velocity $v_r(r_g)$ in Eq. (37). We find that the gas velocity is nearly constant in the neighborhood of r_g and the surface density is near its peak, so the solution is insensitive to the details of this convention.

	§§	$\dot{M}\partial_r(r^2\Omega)$	T_ν	$\partial_r T_d$
Far zone	4.1.1	✓	$\varphi(r, r_{\text{ISCO}})$	0
Mid. <i>with gap</i>	4.1.3	0	$T_{\text{bc}}^{\text{mg}}(r_s, r_g)$	0
Mid. <i>overflow</i>	4.1.2	0	$T_{\text{bc}}^{\text{mo}}(r_s, r_i)$	0
Near <i>ext. uns.</i>	4.2.2	0	$\zeta(r, r_s, r_i)$	$r_s^4/ \delta r ^4$
Near <i>ext. sat.</i>	4.2.3	0	$\psi(r, r_s, r_i)$	r_s^4/H^4
Near interior	4.2.1	✓	0	$-r^4/ \delta r ^4$

Table 1. Approximations and notations for the various radial zones in the disk, used in § 4.

and shows which terms are relevant in Eq. (11). The subdominant terms are marked with a “0”. The column with T_ν shows functions we introduced related to the viscous torque, and $\partial_r T_d$ shows the scaling of the specific tidal torque in Eq. (5).

In the following we mostly focus on β -disks (i.e. $b = 1$) and examine both radiation and gas pressure dominated disks, but it is straightforward to derive analogous formulas for α -disks in the same way. We also note that in the radiation-pressure dominated regime, the viscosity of α -disks is larger by a factor of $p_{\text{gas}}/(p_{\text{gas}} + p_{\text{rad}}) = \beta^{-1}$. This would generally lead to stronger overflows for a smaller gas pile-up, and the cavity would close for a wider range of parameters than we find below for β disks.

4.1 Far and middle zones

First we examine the region sufficiently far from the secondary, either inside or outside of its orbit, where

$$|\partial_r T_d| \ll \partial_r T_\nu \approx \dot{M}\partial_r(r^2\Omega). \quad (26)$$

In this region, Eq. (11) can be integrated and substituted in (18)

$$T_\nu = \dot{M}r^2\Omega + T_{\text{bc}}, \quad (27)$$

$$F \approx D_\nu = \frac{3}{8\pi} \frac{\Omega}{r^2} T_\nu = \frac{3}{8\pi} \left[\dot{M}\Omega^2 + T_{\text{bc}} \frac{\Omega}{r^2} \right], \quad (28)$$

where T_{bc} is an integration constant determined by the boundary condition near the secondary. For a fixed T_{bc} , Eq. (28) gives both F and D_ν , from which the surface density and central temperature follow from Eqs. (21–22),

$$\Sigma = \frac{8^{2/5} (\mu m_p/k)^{4/5} \sigma^{1/5} \beta^{(1-b)/5}}{(9\pi)^{3/5} \alpha^{4/5} \kappa^{1/5}} \frac{\Omega^{(1-b)/5}}{\Omega^{4/5}} \left[\dot{M}\Omega^2 + T_{\text{bc}} \frac{\Omega}{r^2} \right]^{3/5}, \quad (29)$$

$$T_c = \frac{3^{1/5} (\mu m_p/k)^{1/5} \kappa^{1/5} \beta^{(1-b)/5}}{(8\pi)^{2/5} \alpha^{1/5} \sigma^{1/5}} \frac{\Omega^{(1-b)/5}}{\Omega^{1/5}} \left[\dot{M}\Omega^2 + T_{\text{bc}} \frac{\Omega}{r^2} \right]^{2/5}, \quad (30)$$

where

$$\frac{\beta^{(b+4)/10}}{1-\beta} = \frac{(8\pi)^{4/5} c[k/(\mu m_p)]^{2/5}}{3^{9/10} (\alpha\sigma)^{1/10} \kappa^{9/10}} \frac{\Omega^{9/10}}{\left[\dot{M}\Omega^2 + T_{\text{bc}} \frac{\Omega}{r^2} \right]^{4/5}}. \quad (31)$$

Thus, solving the disk structure in these zones amounts to finding the torque at the boundary, T_{bc} .

If $T_\nu(r_{\text{min}}) = 0$ then Eq. (11) shows that,

$$T_{\text{bc}} = -\dot{M}r_{\text{min}}^2\Omega(r_{\text{min}}) + \int_{r_{\text{min}}}^r \partial_r T_d dr. \quad (32)$$

In practice, $r_{\text{min}} = r_{\text{ISCO}}$ for a disk without a cavity, and it is the inner edge of the disk if it has a cavity. Depending on which term dominates in Eq. (27), we distinguish the far zone ($|T_{\text{bc}}| \ll \dot{M}r^2\Omega$) and the middle zone ($|T_{\text{bc}}| \gg \dot{M}r^2\Omega$). The far zone can be either well inside or far outside the secondary’s orbit, but the middle zone is always outside. Well inside the secondary, the second term can be neglected in Eq. (32), and well outside of it, the second term dominates and the integration domain can be extended to ∞ . In both cases, T_{bc} is independent of r .

Eqs. (27) and (32) show, that in the region outside the secondary, T_{bc} represents a *torque barrier* due to the secondary’s tidal effects. This parameter can also be used to obtain the migration rate of the secondary. Indeed, combining Eqs. (9) and (32) gives

$$v_{\text{sr}} = -\frac{2T_{\text{bc}}}{m_s r_s \Omega_s} - \frac{2T_{\text{GW}}}{m_s r_s \Omega_s}. \quad (33)$$

4.1.1 Far zone – unperturbed disk

Without the secondary Eq. (12) implies that $T_{\text{bc}} = -\dot{M}r_{\text{ISCO}}^2\Omega_{\text{ISCO}}$. Substituting into Eqs. (27–28), gives D_ν and F . Plugging into Eqs. (8), (16), and (21–22) leads to the standard Shakura & Sunyaev (1973) solution

$$\Sigma_0 = 4.7 \times 10^5 \frac{\text{g}}{\text{cm}^2} \alpha_{-1}^{-4/5} \dot{m}_{-1}^{3/5} M_7^{1/5} r_2^{-3/5} \varphi^{3/5} \quad (34)$$

$$T_{c0} = 5.4 \times 10^5 \text{K} \alpha_{-1}^{-1/5} \dot{m}_{-1}^{2/5} M_7^{-1/5} r_2^{-9/10} \varphi^{2/5} \quad (35)$$

$$F_0 = \frac{3}{8\pi} \dot{M}\Omega^2 = 7.9 \times 10^{13} \frac{\text{erg}}{\text{s cm}^2} \dot{m}_{-1} M_7^{-1} r_2^{-3} \varphi \quad (36)$$

$$v_{r0} = -3600 \frac{\text{cm}}{\text{s}} \alpha_{-1}^{4/5} \dot{m}_{-1}^{2/5} M_7^{-1/5} r_2^{-2/5} \varphi^{-3/5}, \quad (37)$$

$$H_0 = \begin{cases} 1.5 M_\bullet \dot{m}_{-1} \varphi & \text{if } \beta \ll 1, \\ 0.28 M_\bullet \alpha^{-1/10} \dot{m}_{-1}^{1/5} M_7^{-1/10} r_2^{21/20} \varphi^{1/5} & \text{if } \beta \sim 1. \end{cases} \quad (38)$$

Here and below, the subscript $_0$ denotes quantities related to the unperturbed disk, $\alpha_{-1} = \alpha/0.1$, $\dot{m}_{-1} = (\dot{M}/\dot{M}_{\text{Edd}})/0.1$, \dot{M}_{Edd} is the Eddington accretion rate for 10% radiative efficiency, $q_{-3} = q/10^{-3}$, $M_7 = M_\bullet/10^7 M_\odot$, $r_{s2} = r_s/10^2 M_\bullet$, and we introduced

$$\varphi \equiv 1 - r_{\text{ISCO}}^2 \Omega_{\text{ISCO}} / (r^2 \Omega) = 1 - (r_{\text{ISCO}}/r)^{1/2}. \quad (39)$$

Without the secondary, in the radiation pressure dominated regime ($\beta \ll 1$) the scale-height is approximately constant, and increases approximately linearly further out where gas pressure dominates ($\beta \sim 1$).

The viscous torque, for future reference:

$$T_{\nu 0} = \dot{M}r^2\Omega\varphi = 7.1 \times 10^{47} \text{erg } \dot{m} M_7^2 r_2^{1/2} \varphi, \quad (40)$$

where $r_2 = r/10^2 M_\bullet$. Sufficiently far from the secondary, the disk is independent of the secondary and follows Eqs. (34–38) with $\varphi \approx 1$. However, the disk structure depends on the rate at which gas is allowed to flow in through \dot{M} .

4.1.2 Middle zone

Now let us consider the opposite limit, $T_{\text{bc}} \gg \dot{M}r^2\Omega$, where the steady-state perturbation to the torque is significant. In terms of the dimensionless torque barrier,

$$k = \frac{T_{\text{bc}}}{\dot{M}r^2\Omega} \equiv k_s \frac{r_s^2 \Omega_s}{r^2 \Omega}, \quad (41)$$

the formulae describing the unperturbed disk, Eq. (34–38), get modified by replacing the boundary term with

$$\varphi \rightarrow 1 + k. \quad (42)$$

The disk quantities change to

$$\Sigma^{\text{m}} = \left(\frac{k+1}{\varphi} \right)^{3/5} \Sigma_0 \propto r^{-9/10} \quad (43)$$

$$T_c^{\text{m}} = \left(\frac{k+1}{\varphi} \right)^{2/5} T_{c0} \propto r^{-11/10} \quad (44)$$

$$F^{\text{m}} = \left(\frac{k+1}{\varphi} \right) F_0 \propto r^{-7/2} \quad (45)$$

$$v_r^{\text{m}} = \left(\frac{k+1}{\varphi} \right)^{-3/5} v_{r0} \propto r^{-1/10} \quad (46)$$

$$H^{\text{m}} = \begin{cases} (k+1)H_0/\varphi \propto r^{-1/2} & \text{if } \beta \ll 1, \\ ((k+1)/\varphi)^{1/5} H_0 \propto r^{19/20} & \text{if } \beta \sim 1. \end{cases} \quad (47)$$

and the migration rate follows from Eq. (33)

$$v_{\text{sr}} \approx -\frac{2T_{\text{bc}}}{m_s r_s \Omega_s} = -2k_s \frac{\dot{M} r_s}{m_s} \quad (48)$$

where we have assumed $T_{\text{GW}} \ll T_{\text{bc}}$. Here and below, the superscript “m” labels the middle zone. Note that the dimensionless angular momentum flux k can be interpreted as a *brightening factor* in the middle zone relative to the unperturbed disk; k_s is representative of the maximum brightening, if $k(r)$ is extrapolated to r_s . In practice, the maximum brightening is even larger than k_s in the near zone due to tidal heating (see § 4.3 below).

The disk is modified within a radial range where the dimensionless angular momentum flux satisfies $k > 1$. This sets the outer boundary r_f^{m} of the middle zone, where the disk transitions to the far zone. From Eq. (41),

$$r_f^{\text{m}} = \frac{T_{\text{bc}}^2}{GM_* \dot{M}^2} = k_s^2 r_s. \quad (49)$$

Eqs. (43–47) represent a disk with negligible inflow of angular momentum but an inner boundary condition with a large viscous torque, corresponding to the torque barrier. Such solutions are often (somewhat misleadingly) referred to as a *decretion disk* (Pringle 1991; Lodato et al. 2009). To avoid confusion, we emphasize that there is accretion (i.e. inflow) in this region, too, with a fixed \dot{M} . However, the radial accretion velocity is greatly reduced, while the surface density, temperature, and scale-height are all greatly increased, relative to an accretion disk around a single compact object.

So far in this subsection, we have derived a solution for an arbitrary torque barrier or k , without specifying its value. In general, k is given by Eq. (32), which depends on the tidal torque in the near zone. Thus, to complete the derivation of the disk structure in the middle zone, we are first required to obtain the disk structure in the near zone (which we will do in § 4.2 below). However, in the case of the steady-state cavity, the particular form of the boundary condition allows us to directly infer k , independently of the near zone, up to a factor λ of order unity, which we show next.

4.1.3 Middle zone – steady-state disk with a cavity

When the tidal torque is sufficiently strong to clear a gap so that the secondary and the nearby gas move with a similar

velocity, $T_\nu \sim T_{\text{bc}}$ can be substantial over a large range of radii. From Eq. (13–14), this requires

$$T_\nu^{\text{mg}} = T_{\text{bc}}^{\text{mg}} = \int_0^\infty \partial_r T_{\text{d}} dr = \frac{m_s r_s^2 \Omega_s \dot{M}}{4\pi r_s^2 \Sigma(r_g)}. \quad (50)$$

Here and below, the superscript ^g refers to solutions with a gap, and $r_g = \lambda r_s$ is the outer radius of the gap. For this value of T_{bc} , Eq. (28) gives F and D_ν , and Σ follows from (21). However, since the right hand side (RHS) of Eq. (50) depends on Σ itself, this gives an algebraic equation for T_{bc} . The solution is

$$T_{\text{bc}}^{\text{mg}} = \frac{3^{3/4} \alpha^{1/2} \kappa^{1/8}}{4\pi^{1/4} (\mu m_p / k)^{1/2} \sigma^{1/8}} m_s^{5/8} \dot{M}^{5/8} \frac{\Omega_s^{3/4} r_s^{3/4}}{\lambda^{11/16}} \quad (51) \\ = 1.6 \times 10^{49} \text{ erg } \alpha_{-1}^{1/2} \dot{m}_{-1}^{5/8} \lambda^{-11/16} q_{-3}^{5/8} M_7^{5/4} r_{s2}^{-3/8}.$$

Note that this is independent of the tidal torque model (i.e. the Λ or f in Eq. (5)), since here the tidal torque is set by the boundary condition of the gap. This solution breaks down, and becomes tidal torque dependent, if the gap closes, which we discuss in § 4.2 below.

The dimensionless angular momentum flux from Eq. (41) is

$$k^{\text{mg}} = 23 \alpha_{-1}^{1/2} \dot{m}_{0.1}^{-3/8} M_7^{-3/4} q_{-3}^{5/8} \lambda^{-19/16} r_{s2}^{-7/8} \left(\frac{r}{\lambda r_s} \right)^{-1/2}. \quad (52)$$

In particular, near the secondary $k^{\text{mg}}(r_s) = m_s / (4\pi r_g^2 \Sigma_g)$ is the ratio of secondary mass to the accumulated local gas mass.¹⁴ The only free parameter in this zone is λ , which we determine explicitly in § 4.3.2 below.

In the range $r_s \ll r \ll r_f^{\text{mg}}$, $k^{\text{mg}} \gg 1$ and Eqs. (43–47) give

$$\Sigma^{\text{mg}} = 3.1 \times 10^6 \frac{\text{g}}{\text{cm}^2} \frac{\dot{m}_{-1}^{3/8}}{\alpha_{-1}^{1/2}} \frac{q_{-3}^{3/8}}{M_7^{1/4}} \lambda^{-33/80} r_{s2}^{-9/40} r_2^{-9/10}, \quad (53)$$

$$T_c^{\text{mg}} = 1.9 \times 10^6 \text{ K } \dot{m}_{-1}^{1/4} \frac{q_{-3}^{1/4}}{M_7^{1/2}} \lambda^{-11/40} r_{s2}^{-3/20} r_2^{-11/10}, \quad (54)$$

$$v_r^{\text{mg}} = \lambda v_{\text{sr}} \left(\frac{r}{\lambda r_s} \right)^{-1/10} \quad (55)$$

$$H^{\text{mg}} = \begin{cases} 35 M_\bullet \alpha_{-1}^{1/2} \dot{m}_{-1}^{5/8} M_7^{-3/4} \lambda^{-19/16} q_{-3}^{5/8} r_{s2}^{-7/8} \\ \quad \times (r/\lambda r_s)^{-1/2} & \text{if } \beta \ll 1, \\ 0.53 M_\bullet \dot{m}_{-1}^{1/8} M_7^{-1/4} \lambda^{-11/16} q_{-3}^{1/8} r_{s2}^{-3/40} r_2^{19/20} & \text{if } \beta \sim 1. \end{cases} \quad (56)$$

where $\Sigma(r) \sim 0$ at $r \leq \lambda r_s$. Outside $r \gg r_f^{\text{mg}}$, $k^{\text{mg}} \approx 0$, and the disk approaches the unperturbed solution given by Eqs. (34–38). In the transition zone, between the middle and far zones, $r \sim r_f^{\text{mg}}$, one needs to use Eqs. (43–47) with $k = k^{\text{mg}}$ (Eq. 52).

When a cavity is present, the migration speed of the secondary follows from Eqs. (33) and (51):

$$v_{\text{sr}}^{\text{g}} = -550 \frac{\text{cm}}{\text{s}} \alpha_{-1}^{1/2} \dot{m}_{-1}^{5/8} M_7^{1/4} q_{-3}^{-3/8} \lambda^{-11/16} r_{s2}^{1/8}. \quad (57)$$

¹⁴ Here $k^{\text{mg}}(r_s) = B^{-5/8}$ using the Syer-Clarke parameter $B = m_s / (4\pi r_s^2 \Sigma_{s0})$.

This expression is consistent with the secondary dominated Type-II migration rate of Syer & Clarke (1995) who assumed $\lambda = 1$. Note that the migration speed is slower than the gas inflow velocity without the secondary, $|v_{\text{sr}}^{\text{mg}}| < |v_{r0}(r_s)|$ in Eq. (37). This is referred to as disk-dominated Type-II migration, which is appropriate if the secondary mass is smaller than the unperturbed local disk mass $m_s \leq 4\pi r_g^2 \Sigma_0(r_g)$ (or equivalently $k^{\text{mg}} \geq 1$), but large enough to open a gap.

It is interesting to note that the structure of the middle zone does not depend explicitly on the tidal torque model, $\partial_r T_d$ (in particular Λ or the f_2 parameter in Eq. 5); the dependence is implicit and arises only by fixing the value of λ . Physically, while the tidal torques are negligible in this region, the effects of the tidal torques are still communicated to the region by setting an effective hydrodynamical boundary condition. We determine λ in § 4.3.2 below and find that, in fact, it only weakly depends on $\partial_r T_d$.

4.1.4 Consistency of steady-state

A basic assumption of our model is that the radial structure of the disk is in a quasi steady-state as the secondary migrates slowly inwards. To check the consistency of these steady-state solutions, we must verify that the implicit time-dependence in the surface density profile through $r_s(t)$ does not violate the continuity equation (1) significantly, so that

$$\partial_r \dot{M} = -\partial_r (2\pi r \Sigma v_r) = -2\pi r \partial_t \Sigma \stackrel{?}{=} 0 \quad (58)$$

Integrating over radius, the relative error in the accretion rate

$$\frac{\int 2\pi r \dot{\Sigma}^{\text{mg}} dr}{\dot{M}} = \frac{\int 2\pi r v_{\text{sr}}^{\text{mg}} \partial_{r_s} \Sigma^{\text{mg}} dr}{2\pi r v_r^{\text{mg}} \Sigma^{\text{mg}}} = \frac{9}{44} \left(\frac{r}{\lambda r_s} \right)^{11/10} \quad (59)$$

which is $\sim 20\%$ near the gap edge. The error in T_{bc} based on Eq. (51) is $\sim 13\%$. However, the error in the accretion rate exceeds unity at large radii, outside $4.2\lambda r_s$. The steady-state assumption breaks down because as the secondary migrates inward, the steady-state gas density near the edge of the gap continuously increases with time. If \dot{M} is fixed near the gap edge to be a constant fraction of the Eddington value, the true accretion rate $\dot{M}(r)$ at larger radii must be larger, to supply material for the increasing gas density. Conversely, if $\dot{M}(r)$ is fixed at large radii, then it becomes smaller approaching the gap edge. Such non-steady-state solutions have been derived by Pringle (1991) and Ivanov et al. (1999) by solving the nonlinear diffusion equation (7) for a fixed outer boundary condition, assuming that the viscosity can be expressed as $\nu = k\Sigma^a r^b$ where k , a , and b are constants. In particular, Ivanov et al. (1999) derived a non-steady, but self-similar solution. In that solution, the migration is slower, and the angular momentum flux is lower, compared to the Syer & Clarke (1995) steady-state solutions with a fixed \dot{M} for the same binary and disk parameters (Syer & Clarke 1995). The quasi-steady migration rate and brightening factors for a truncated disk with $\lambda > 1$ are intermediate between the Syer & Clarke (1995) and Ivanov et al. (1999) solutions.

The steady-state condition is typically *not* violated in

the overflowing solution over a wide radial range. For global-steady state, a necessary condition is

$$\left| \frac{\int_0^{r_g} 2\pi r \dot{\Sigma}^{\text{mg}} dr}{\dot{M}} \right| = \left| \frac{\gamma_{\Sigma_s}}{2 + \gamma_{\Sigma_r}} \right| k_s^{19/5} \frac{4\pi r_s^2 \Sigma_0(r_s)}{m_s} \ll 1 \quad (60)$$

where we have used Eqs. (29), (48), and (49) and defined $\gamma_{\Sigma_s} = \partial \ln \Sigma^{\text{mg}} / \partial \ln r_s$ and $\gamma_{\Sigma_r} = \partial \ln \Sigma^{\text{mg}} / \partial \ln r$. This sets a maximum limit for the dimensionless angular momentum flux k_s . For a β -disk, this implies

$$k_{s \text{ max}} = 3.2 |\gamma_{\Sigma_s}|^{5/19} \alpha_{-1}^{4/19} \dot{m}_{-1}^{-3/19} M_7^{6/19} q_{-3}^{5/19} r_{s2}^{-7/19}, \quad (61)$$

and $k_{s \text{ max}}$ is larger (i.e. less restrictive) for radiation pressure dominated α -disks.

An important qualitative difference between the overflowing model presented here and the Syer & Clarke (1995) model for a truncated disk is that $\gamma_{\Sigma_s} > 0$ for the former as we show below. In contrast, in the overflowing case, the excess surface density and the dimensionless angular momentum flux k_s in the middle zone both gradually decrease during the inward migration of the secondary. Thus, the excess surface density diffuses radially outwards. If $k_s < k_{s \text{ max}}$ then the diffusion is sufficiently fast to reach a global quasi-steady-state throughout the middle zone. If this is not satisfied, then the outer parts of the middle zone cannot respond as quickly as the object moves inwards and the structure of the disk in these regions will depend on its previous history. However, since the viscous timescale is always much smaller than the migration timescale in at least the inner parts of the middle zone, the local disk structure of the overflowing solution might approach an approximate steady-state there with a constant \dot{M} even if $k_s \gtrsim k_{s \text{ max}}$. The migration rate of the secondary depends on the near-zone of the disk, which is expected to remain insensitive to perturbations in the outer parts of the middle zone in an overflowing disk.¹⁵ We leave a detailed investigation of the time dependent overflowing solutions to future work (Salem et al. 2012, in preparation).

4.2 Near zone

Now let us consider the regions near the secondary where the tidal torque and heating are important. We discuss steady-state solutions inside and outside of the secondary's orbit, in turn, without and then with a circular cavity. Deriving the physical properties of the disk in this region is useful to provide an estimate of the torque barrier, T_{bc} , at the interface between the near zone and the middle zone. As explained previously, the torque barrier sets the overall scale of the physical properties in the middle zone, as well as the migration rate of the secondary. We therefore first compute the value of the torque barrier for an overflowing disk, as well as for a disk with a wide gap. In the latter case, we then compare the value with the torque barrier in the middle zone derived above (Eq. 51). By equating the two, we can estimate the gap size (i.e. λ), and obtain the conditions for gap opening and closing.

¹⁵ This is different from a transient truncated circumbinary disk where the migration velocity is comparable to the local gas accretion velocity, which can exhibit hysteresis throughout the middle zone (Rafikov 2012).

4.2.1 Inside the secondary orbit

Consider the region just downstream the secondary, outside the torque cutoff $\Delta = r_s - r > H$ in Eq. (6), assuming a steady-state overflow (i.e. no hollow circular cavity). Based on Eq. (11), the viscous torque decreases in the vicinity of the secondary and for a sufficiently large secondary mass, the angular momentum exchange is dominated by the tidal torque. In this regime,

$$|\partial_r T_\nu| \ll |\partial_r T_d| = 2\pi r |\Lambda| \Sigma \approx \dot{M} \partial_r (r^2 \Omega) \quad (62)$$

implying that

$$\Sigma^{\text{ni}} = \frac{\dot{M}}{4\pi} \frac{\Omega}{|\Lambda|} = \frac{\dot{M}}{2\pi f q^2} \frac{1}{r^2 \Omega} \frac{\Delta^4}{r^4} \quad (63)$$

for a Keplerian disk (here and below, the superscript $^{\text{ni}}$ refers to the solutions in the inner near zone). Eq. (20) shows that

$$F^{\text{ni}} \approx D_d = \frac{1}{2} (\Omega_s - \Omega) \Lambda \Sigma = \frac{\dot{M}}{8\pi} \Omega (\Omega - \Omega_s) \rightarrow \frac{F_0}{2} \frac{\Delta}{r}. \quad (64)$$

The asymptotic limit corresponds to $\Delta \ll r$. From Eqs. (8) and (16)

$$\begin{aligned} v_r^{\text{ni}} &= \frac{2\Lambda}{r\Omega} = f q^2 \frac{r^5 \Omega}{\Delta^4} \quad (65) \\ H^{\text{ni}} &= \frac{\kappa \dot{M}}{8\pi c} \frac{\Omega - \Omega_s}{\Omega} \rightarrow \frac{H_0}{2} \frac{\Delta}{r} \quad \text{if } \beta \sim 1 \quad (66) \end{aligned}$$

The latter equation shows that the secondary makes the disk thinner downstream if the disk is radiation pressure dominated. Combining Eqs. (63–64) with (21), gives D_ν^{ni} . The viscous torque then follows from Eq. (18). To first beyond leading order, for $b = 1$,

$$\begin{aligned} T_\nu^{\text{ni}} &= 2.4 \times 10^{50} \text{erg} \alpha_{-1} \dot{m}_{-1}^{3/2} f_{-2}^{-5/4} M_7^{7/4} q_{-3}^{-5/2} \\ &\times r_2^{5/8} \left(\frac{r}{r_s}\right)^{5/16} \left(\frac{\Delta}{r}\right)^{21/4}, \quad (67) \end{aligned}$$

T_ν^{ni} exhibits a sharp cutoff near the secondary.

We can verify that the working assumptions hold in this region. Eq. (66) shows that $\Delta > H$ holds for all Δ , since the unperturbed disk is thin, $H_0 < r$. Since $D_\nu^{\text{ni}} \propto T_\nu^{\text{ni}} \propto \Delta^{21/4}$ which implies that $D_\nu^{\text{ni}} \ll F^{\text{ni}}$ is indeed satisfied for sufficiently small Δ . Coincidentally, the assumption in Eq. (62) is satisfied within a distance Δ_{ni} from the secondary, where

$$\frac{\Delta_{\text{ni}}}{r_s} = \frac{x_{\text{ni}}}{1 + \frac{841}{714} x_{\text{ni}}} \quad (68)$$

and

$$x_{\text{ni}} = 0.1 \alpha_{-1}^{-4/17} \dot{m}_{-1}^{-2/17} M_7^{1/17} f_{-2}^{5/17} q_{-3}^{10/17} r_{s2}^{-1/34}. \quad (69)$$

The disk parameters in the region $r_s - \Delta^{\text{ni}} \lesssim r \lesssim r_s - r_H$

are

$$\Sigma^{\text{ni}} = 5.7 \times 10^7 \frac{\text{g}}{\text{cm}^2} f_{-2}^{-1} \dot{m}_{-1} q_{-3}^{-2} r_2^{-1/2} (\Delta/r)^4, \quad (70)$$

$$\begin{aligned} T_c^{\text{ni}} &= 1.5 \times 10^6 \text{K} f_{-2}^{-1/4} \dot{m}_{-1}^{1/2} M_7^{-1/4} q_{-3}^{-1/2} r_2^{-7/8} \\ &\times \left(\frac{r}{r_s}\right)^{5/16} \left(\frac{\Delta}{r}\right)^{5/4}, \quad (71) \end{aligned}$$

$$F^{\text{ni}} = 3.9 \times 10^{13} \frac{\text{erg}}{\text{s cm}^2} \dot{m}_{-1} M_7^{-1} r_2^{-3} \left(\frac{r}{r_s}\right)^{5/4} \frac{\Delta}{r}, \quad (72)$$

$$v_r^{\text{ni}} = 30 \frac{\text{cm}}{\text{s}} f_{-2} q_{-3}^2 r_2^{-1/2} (\Delta/r)^{-4}, \quad (73)$$

$$H^{\text{ni}} = \begin{cases} 0.75 M_\bullet \dot{m}_{-1} (r/r_s)^{5/4} (\Delta/r) & \text{if } \beta \ll 1, \\ 0.36 M_\bullet f_{-2}^{-1/8} \dot{m}_{-1}^{1/4} M_7^{-1/8} q_{-3}^{-1/4} r_2^{17/16} \\ \times (r/r_s)^{5/32} (\Delta/r)^{5/8} & \text{if } \beta \sim 1. \end{cases} \quad (74)$$

During the inward migration of the secondary, r_s decreases, and the surface density evolves in a self-similar way. The surface density, midplane temperature, surface brightness, and scale-height all decrease significantly near the secondary with large q_{-3} . The radial flow velocity becomes very large in the close vicinity, and the flow may become advection dominated there. However, we do not extrapolate this solution inside the Hill radius of the secondary because the torque model is invalid there.

It is remarkable that for a fixed \dot{M} , the fractional perturbation to the surface brightness and the radiation-pressure-dominated scale-height are universal in this region, independent of the binary and disk parameters. This property is general for an arbitrary torque or viscosity model in radiatively efficient steady-state disks. The surface density in this regime is also independent of the viscosity model but it is sensitive to the torque model: it is set to ensure that the tidal torque matches the angular momentum flow associated with \dot{M} . The original value of the surface density is suppressed by a factor proportional to $q^{-2} \Delta$. These solutions are valid only for disks with relatively large secondary masses, such that $\Delta_{\text{ni}} > r_H$, but in which there is gas inflow across the secondary orbit.

4.2.2 Outside the secondary – unsaturated torque

Next consider the region just outside the secondary. Here we examine the case where the secondary is massive enough for the tidal torques to be important. After a significant amount of gas pile-up the viscous torque eventually counteracts the tidal torque and creates a stationary inflow. In this regime the tidal and viscous torques counteract one another and both greatly exceed the momentum flux in Eq. (11) such that

$$\dot{M} \partial_r (r^2 \Omega) \ll \partial_r T_\nu \approx \partial_r T_d = 2\pi r \Lambda \Sigma. \quad (75)$$

The tidal heating rate is much larger than the viscous heating rate of a disk without a satellite, making the disk much hotter and thicker. Let us assume $D_d \gg D_\nu$ here, Eq. (20) implying that

$$F \approx D_d = \frac{1}{2} (\Omega_s - \Omega) \Lambda \Sigma. \quad (76)$$

In this subsection we examine the case where the torque is not saturated, $H(r) < r - r_s$, so that $\Delta = r - r_s$ in Eq. (6). This is most relevant for relatively small mass ratios, (i.e. typically $q \lesssim 10^{-3}$, see Eq. 95 below and Paper II), where the

banking up of the stream in this region is modest. Substitute Eq. (21) for Σ with $b = 1$, and use Eq. (18),

$$F = \left(\frac{3}{8\pi}\right)^{4/5} \frac{a_\Sigma}{2} (\Omega_s - \Omega) \Lambda r^{-2/5} \frac{T_\nu^{4/5}}{F^{1/5}} \quad (77)$$

where a_Σ is the constant coefficient in Eq. (21). Solve this for F and plug back into Eq. (76)

$$\frac{\partial_r T_\nu}{T_\nu^{2/3}} = \frac{2^{13/19} \pi^{13/15}}{3^{2/15} a_\Sigma^{1/6}} \frac{r \Lambda^{5/6}}{(\Omega_s - \Omega)^{1/6}} \quad (78)$$

Integrating both sides between r_i , the inner edge of this region (see further below for a discussion of the value of r_i) and r ,

$$T_\nu^{1/3}(r) - T_\nu^{1/3}(r_i) = \frac{2^{13/19} \pi^{13/15}}{3^{17/15} a_\Sigma^{1/6}} \int_{r_i}^r \frac{r \Lambda^{5/6}}{(\Omega_s - \Omega)^{1/6}} dr. \quad (79)$$

We are most interested in the case where the tidal torques increase T_ν substantially in this region. If so, we approximate $T_\nu(r_i) = 0$. Substituting Eq. (5), and rearranging gives

$$T_\nu^{\text{neu}} = 3.5 \times 10^{40} \text{ erg } \alpha_{-1}^{-2} M_7^{5/2} f_{-2}^{5/2} q_{-3}^5 r_{s2}^{1/4} \zeta^3(r, r_s, r_i) \quad (80)$$

where the superscript $^{\text{neu}}$ refers to the case of unsaturated torque in the external near zone, and

$$\begin{aligned} \zeta &\equiv \int_{r_i/r_s}^{r/r_s} x^{-7/6} (1 - x^{-3/2})^{-1/6} (x - 1)^{-10/3} dx \quad (81) \\ &\approx \left(\frac{2}{3}\right)^{1/6} \frac{2}{5} \frac{(r_i/r_s)^{-115/72}}{(\Delta_i/r_s)^{5/2}} \left[1 - \left(\frac{r_i}{r}\right)^{115/72} \left(\frac{\Delta_i}{\Delta}\right)^{5/2}\right]. \end{aligned}$$

In the second line, the approximation is accurate to within 6% for $\Delta_i \equiv r_i - r_s \leq 0.3 r_s$. Note that T_ν^{neu} depends on radius only through ζ ; it increases monotonically and approaches a constant value, which depends very sensitively on Δ_i/r_s . In practice, one might expect

$$\Delta_i \sim r_H \quad \text{and} \quad r_i = r_s + r_H \quad (82)$$

for a disk without a cavity because the tidal torque model is valid only outside this region, and within this distance the gas may flow across the secondary orbit along radial streams or horse shoe orbits. In the following we keep Δ_i/r_H general. We incorporate a factor of $(r_H/r_s)^{-5/2}$ in the prefactor of Eq. (80) and introduce a renormalized ζ , as

$$\begin{aligned} \zeta_R &\equiv \left(\frac{r_H}{r_s}\right)^{5/2} \zeta \quad (83) \\ &\approx \left(\frac{2}{3}\right)^{1/6} \frac{2}{5} \frac{(r_i/r_s)^{-115/72}}{(\Delta_i/r_H)^{5/2}} \left[1 - \left(\frac{r_i}{r}\right)^{115/72} \left(\frac{\Delta_i}{\Delta}\right)^{5/2}\right]. \end{aligned}$$

Then Eq. (80) becomes

$$\begin{aligned} T_\nu^{\text{neu}} &= 1.7 \times 10^{49} \text{ erg } \alpha_{-1}^{-2} M_7^{5/2} f_{-2}^{5/2} q_{-3}^{5/2} r_{s2}^{1/4} \zeta_R^3 \quad (84) \\ &\approx T_{\nu \text{max}}^{\text{neu}} \times \left[1 - \left(\frac{r_i}{r}\right)^{115/72} \left(\frac{\Delta_i}{\Delta}\right)^{5/2}\right]^3 \end{aligned}$$

where

$$\begin{aligned} T_{\nu \text{max}}^{\text{neu}} &\equiv \lim_{r \rightarrow \infty} T_\nu^{\text{neu}}(r, r_s, r_i) \quad (85) \\ &\approx 9.1 \times 10^{47} \text{ erg } \alpha_{-1}^{-2} M_7^{5/2} f_{-2}^{5/2} q_{-3}^{5/2} r_{s2}^{1/4} \\ &\quad \times \left(\frac{\Delta_i}{r_H}\right)^{-15/2} \left(1 + \frac{\Delta_i}{r_s}\right)^{-115/24}. \quad (86) \end{aligned}$$

The outer edge of this region is where Eq. (75) is first violated, i.e. where the viscous torque density¹⁶ becomes comparable to the accretion term $\partial_r T_\nu \sim \dot{M} \partial_r (r^2 \Omega)$. We substitute $\partial_r T_\nu$ from Eq. (78) utilizing (80) and get

$$\begin{aligned} 1 &= \frac{\partial_r T_\nu^{\text{neu}}}{\dot{M} \partial_r (r^2 \Omega)} = 2.8 \times 10^{-7} \alpha_{-1}^{-2} \dot{m}_{-1}^{-1} M_7^{1/2} f_{-2}^{5/2} q_{-3}^5 r_{s2}^{-1/4} \\ &\quad \times \left(\frac{r}{r_s}\right)^{-11/24} \left(\frac{\Delta}{r_s}\right)^{-7/2} \zeta(r, r_s, r_i)^2. \quad (87) \end{aligned}$$

We label the radial distance of this interface from the secondary as Δ_m^{neu} . While this equation of a single variable can be easily solved numerically for Δ_m^{neu} for any fixed r_s and Δ_i , we may derive an analytical approximate solution as follows. Assuming $1 \gg \Delta_m^{\text{neu}} \gtrsim 3\Delta_i$, ζ is close to its asymptotic maximum, which implies

$$\begin{aligned} \frac{\Delta_m^{\text{neu}}}{\Delta_i} &= 5.0 \alpha_{-1}^{-4/7} \dot{m}_{-1}^{-2/7} M_7^{1/7} f_{-2}^{5/14} q_3^{13/21} r_{s2}^{-1/14} \\ &\quad \times \frac{[1 + (\Delta_i/r_s)]^{-115/126}}{(\Delta_i/r_H)^{17/7}}. \quad (88) \end{aligned}$$

To obtain the dependence of the physical parameters on radius, we first derive D_ν and F by substituting Eq. (84) into (18) and (77). Then Σ and T_c follow from Eqs. (21) and (22). In the range $r_i \leq r \lesssim r_s + \Delta_m^{\text{neu}}$,

$$\begin{aligned} \Sigma^{\text{neu}} &= 1.0 \times 10^7 \frac{\text{g}}{\text{cm}^2} \alpha_{-1}^{-2} f_{-2}^{3/2} M_7^{1/2} q_{-3}^{4/3} r_{s2}^{-3/4} \left(\frac{r}{r_s}\right)^{-23/24} \\ &\quad \times \left(\frac{\Delta}{r_s}\right)^{1/2} \zeta_R^2, \quad (89) \end{aligned}$$

$$T_c^{\text{neu}} = 6.3 \times 10^6 \text{ K } \alpha_{-1}^{-1} f_{-2} r_{s2}^{-1} q_{-3}^{7/6} \left(\frac{r}{r_s}\right)^{-25/24} \left(\frac{\Delta}{r_s}\right)^{-1/2} \zeta_R, \quad (90)$$

$$\begin{aligned} F^{\text{neu}} &= 6.8 \times 10^{12} \frac{\text{erg}}{\text{cm}^2 \text{ s}} \alpha_{-1}^{-2} f_{-2}^{5/2} q_{-3}^{10/3} M_7^{-1/2} r_{s2}^{-13/4} \\ &\quad \times \left(\frac{r}{r_s}\right)^{-77/24} \left(\frac{\Delta}{r_s}\right)^{-5/2} \zeta_R^2, \quad (91) \end{aligned}$$

$$\begin{aligned} v_r^{\text{neu}} &= 173 \frac{\text{cm}}{\text{s}} \alpha_{-1}^2 \dot{m}_{-1} f_{-2}^{-3/2} M_7^{-1/2} q_{-3}^{-4/3} r_{s2}^{-1/4} \left(\frac{r}{r_s}\right)^{-1/24} \\ &\quad \times \left(\frac{\Delta}{r_s}\right)^{-1/2} \zeta_R^{-2}, \quad (92) \end{aligned}$$

$$H^{\text{neu}} = \begin{cases} 0.13 M_\bullet \alpha_{-1}^{-2} f_{-2}^{5/2} M_7^{1/2} r_{s2}^{-1/4} (r/r_s)^{-5/24} \\ \quad \times (\Delta/r_s)^{-5/2} \zeta_R^2 \quad \text{if } \beta \approx 0, \\ 0.23 M_\bullet \alpha_{-1}^{-1/2} f_{-2}^{1/2} r_{s2} (r/r_s)^{47/48} (\Delta/r_s)^{-1/4} \zeta_R^{1/2} \\ \quad \text{if } \beta \approx 1. \end{cases} \quad (93)$$

Here $r = r_s + \Delta$, and these equations are formally correct to first beyond leading order in Δ/r_s , but we find them to be a good approximation typically within 15% even for $\Delta/r_s \gtrsim 1$. Interestingly, all of these physical parameters have a local extremum in this zone. We label the distance corresponding to the maximum local disk luminosity $4\pi r^2 F(r)$ as $\Delta_{\text{peak}}^{\text{neu}}$. We find that $\Delta_{\text{peak}}^{\text{neu}}/\Delta_i$ is a slowly decreasing function of Δ_i , which varies between 1.55 and 1.4 for $0 < \Delta_i \lesssim r_s$.

¹⁶ Note that matching the derivatives at the interface does not contradict $T_\nu^{\text{neu}} \gg \dot{M} r^2 \Omega$ there.

To match T_ν at a radius $r = r_s + \Delta_m^{\text{neu}}$, the interface between this region and the middle zone, we must set $T_{\text{bc}} \equiv T_\nu^{\text{neu}}(r_m^{\text{neu}})$. Based on Eqs. (84) we may use

$$T_{\text{bc}} \approx T_{\nu \text{max}}^{\text{neu}} \quad \text{if } \Delta_m^{\text{neu}} \gg \Delta_i. \quad (94)$$

This equation is typically valid in the overflowing case (see Eq. 88), as long as q is large enough that $T_{\nu \text{max}}^{\text{neu}} > T_{\nu 0}(r_s)$ (strongly perturbed solution), but not too large so that $H < r - r_s$. We discuss the solutions if the latter condition is violated in § 4.2.3 below. Comparing Eqs. (40) and (86) shows that the minimum mass ratio to cause a significant gas buildup with unsaturated torques:

$$q_{\text{min}}^{\text{neu}} = 9 \times 10^{-4} \alpha_{-1}^{4/5} \dot{m}_{-1}^{2/5} M_7^{-1/5} f_{-2}^{-1} r_{s2}^{1/10}. \quad (95)$$

For smaller masses, the disk structure is not modified significantly outside the secondary, and one has to use Eq. (67) for the torque at the inner boundary in Eq. (79) with $T_\nu(r_i) = T_\nu^{\text{ni}}(r - r_H)$. We do not show these more general but more complicated expressions here.

We note that the results in this section are sensitive to Δ_i if different from r_H , which sets the distance at which the gas can flow in across the secondary's orbit without significant resistance. While $\Delta_i \sim r_H$ is reasonable based on the horse shoe orbits in the restricted three body problem, we keep it as a free parameter in the following.

4.2.3 Outside the secondary – saturated torque

Here we again assume that Eqs. (75–76) hold, but now examine the case of much higher secondary masses, where the scale-height is increased so much that $H(r) > r - r_s$ and the tidal perturbation enters the torque cutoff regime. We make the simplifying assumption here that $H(r) > r - r_s$ holds throughout the near zone so that the tidal torque in Eq. (5) does not alternate between saturated and unsaturated. It is straightforward to obtain more general solutions, but we find this exclusively saturated OR unsaturated assumption to be an excellent approximation in most cases.

Due to the large torque barrier and tidal heating, the disk in this region is typically radiation pressure dominated, and we accordingly assume $\beta \approx 0$ for the analytical solutions below.

Eqs. (16), (18), and (21) show that $H = \frac{\kappa}{c} \Omega^{-2} F$ and $\Sigma = a_\Sigma r^{-8/5} T_\nu^{4/5} F^{-1/5}$ for $b = 1$, where a_Σ is a constant. Substituting into Eq. (76),

$$F = \left(\frac{3}{8\pi} \right)^{4/5} \frac{a_\Sigma c^4}{4 \kappa^4} f q^2 r_s^4 r^{2/5} \Omega^{10} (\Omega_s - \Omega) \frac{T_\nu^{4/5}}{F^{21/5}}. \quad (96)$$

This equation can be solved for F as a function of r and T_ν . Plugging back into Eq. (75) leads to a separable first order differential equation for T_ν

$$\frac{\partial_r T_\nu}{T_\nu^{2/13}} = a_1 r_s^{9/52} \left(\frac{\Omega_s - \Omega}{\Omega_s} \right)^{-21/26} \left(\frac{\Omega}{\Omega_s} \right)^{25/13} \left(\frac{r}{r_s} \right)^{14/13}, \quad (97)$$

where a_1 is a constant independent of r and r_s . Now use¹⁷ $\Omega/\Omega_s \approx (r/r_s)^{-3/2}$ and integrate both sides assuming $T_\nu(r_i) \approx 0$ for some $r_i \gtrsim r_s$. Here r_i is the radius where

¹⁷ The disk rotates with nearly the local Keplerian angular velocity, but slightly slower due to a radial pressure gradient: $(\Omega_K - \Omega)/\Omega_K \propto H^2/r^2$ see Eq. (78) in Kocsis et al. (2011).

the torque model breaks down, for which we adopt the Hill radius around the secondary $r_i = [1 + (q/3)^{1/3}]r_s$ if a gap does not form. Thus,

$$T_\nu^{11/13}(r) - T_\nu^{11/13}(r_i) = \frac{11}{13} a_1 r_s^{61/52} \psi(r, r_s, r_i), \quad (98)$$

where we introduced a dimensionless function

$$\psi = \frac{2}{3} B\left(\frac{\Omega_s - \Omega}{\Omega_s}; \frac{5}{26}, \frac{7}{13}\right) - \frac{2}{3} B\left(\frac{\Omega_s - \Omega_0}{\Omega_s}; \frac{5}{26}, \frac{7}{13}\right) \quad (99)$$

$$\approx 3.7 \left[\left(\frac{r - r_s}{r} \right)^{5/26} - \left(\frac{r_i - r_s}{r_i} \right)^{5/26} \right] \quad (100)$$

$$\approx 0.4 \ln \frac{r - r_s}{r - r_i}. \quad (101)$$

Here $B(x; a, b) = \int_0^x t^{a-1} (1-t)^{b-1} dt$ is the incomplete beta function, and the last two lines are simple approximations, typically accurate to within 15%. We can now use Eqs. (18) to get D_ν . For $T_\nu(r_i) \approx 0$, after substituting the value of a_1 , Eq. (98) yields

$$T_\nu^{\text{nes}} = 1.1 \times 10^{49} \text{ erg } \alpha_{-1}^{-2/11} f_{-2}^{5/22} q_{-3}^{5/11} M_7^{45/22} r_{s2}^{61/44} \psi^{13/11} \quad (102)$$

$$D_\nu^{\text{nes}} = 1.2 \times 10^{15} \frac{\text{erg}}{\text{cm}^2 \text{s}} \alpha_{-1}^{-2/11} f_{-2}^{5/22} q_{-3}^{5/11} M_7^{-21/22} \times r_{s2}^{-93/44} \left(\frac{r}{r_s} \right)^{-7/2} \psi^{13/11}. \quad (103)$$

Here the superscript ^{nes} refers to the case of saturated torque in the external near zone. Note that T_ν^{nes} depends on radius only through ψ . Close to the inner boundary of this region r_i , it grows quickly with $\delta r/r$ and saturates to a constant at $\delta r/r \sim 1$. This can be understood, since this solution neglects angular momentum flow, the viscous torque is equal to the integrated tidal torque density, and the latter has a cutoff at $\delta r/r \sim 1$. We can verify that $T_\nu^{\text{nes}} \gg T_{\nu 0}$ is indeed satisfied in this region (c.f. Eq. 40) and so the first assumption, Eq. (75), and $T_\nu(r_i) \approx 0$ are well justified.

Can we use the asymptotic maximum of T_ν^{nes} as an estimate of the torque at the outer boundary of this region, to estimate $T_{\text{bc}}^{\text{mo}}$ in the middle zone of an overflowing disk? In many cases no, because the disk transitions to the middle zone much closer $\delta r \ll r_s$, implying that the torque at the outer boundary of this region can be much less than its asymptotic maximum. The outer boundary of this region is where $H = r - r_s$. To figure out exactly where this happens, we proceed to determine the disk structure in this region.

Now Eqs. (103) and (96) give D_ν and F ; all other disk parameters then follow from Eq. (8), (16), and (21–22). The

result within $r_i \leq r \lesssim r_s + H^{\text{nes}}$ is

$$\Sigma^{\text{nes}} = 2.6 \times 10^6 \frac{\text{g}}{\text{cm}^2} \alpha_{-1}^{-10/11} M_7^{5/22} f_{-2}^{3/22} q_{-3}^{3/11} r_{s2}^{-3/44} \times \left(\frac{\Omega_s - \Omega}{\Omega_s} \right)^{-1/26} \left(\frac{r}{r_s} \right)^{-27/26} \psi^{10/11}, \quad (104)$$

$$T_c^{\text{nes}} = 1.6 \times 10^6 \text{K} \alpha_{-1}^{-3/11} M_7^{-2/11} f_{-2}^{1/11} q_{-3}^{2/11} r_{s2}^{-6/11} \times \left(\frac{\Omega_s - \Omega}{\Omega_s} \right)^{1/26} \left(\frac{r}{r_s} \right)^{-25/26} \psi^{3/11}, \quad (105)$$

$$F^{\text{nes}} = 9.8 \times 10^{14} \frac{\text{erg}}{\text{cm}^2 \text{s}} \alpha_{-1}^{-2/11} M_7^{-21/22} f_{-2}^{5/22} q_{-3}^{5/11} r_{s2}^{-93/44} \times \left(\frac{\Omega_s - \Omega}{\Omega_s} \right)^{5/26} \left(\frac{r}{r_s} \right)^{-73/26} \psi^{2/11}, \quad (106)$$

$$v_r^{\text{nes}} = 660 \frac{\text{cm}}{\text{s}} \alpha_{-1}^{10/11} \dot{m}_{-1} M_7^{-5/22} f_{-2}^{-3/22} q_{-3}^{-3/11} r_{s2}^{-41/44} \times \left(\frac{\Omega_s - \Omega}{\Omega_s} \right)^{1/26} \left(\frac{r}{r_s} \right)^{1/26} \psi^{-10/11}, \quad (107)$$

$$H^{\text{nes}} = 19 M_\bullet \alpha_{-1}^{-2/11} M_7^{1/22} f_{-2}^{5/22} q_{-3}^{5/11} r_{s2}^{39/44} \times \left(\frac{\Omega_s - \Omega}{\Omega_s} \right)^{5/26} \left(\frac{r}{r_s} \right)^{5/26} \psi^{2/11}. \quad (108)$$

We can now confirm the consistency of the second assumption, Eq. (76), using Eqs. (103) and (106). Indeed, $D_\nu^{\text{nes}} \lesssim F^{\text{nes}}$ near the secondary since D_ν^{nes} scales with a higher power of ψ . Σ and T_c have a maximum, v_r decreases and becomes practically constant, while H slowly increases in this regime.

The outer boundary of this region, r_m^{nes} , is where¹⁸

$$H^{\text{nes}}(r_m^{\text{nes}}) = \delta r_m^{\text{nes}} \equiv r_m^{\text{nes}} - r_s. \quad (109)$$

We use r_m^{nes} as an approximation to the transition radius to the middle zone. After substituting Eq. (108), Eq. (109) is a nonlinear algebraic equation for r_m^{nes} . While it is easy to solve it numerically for any choice of parameters, it is still useful to derive approximate analytical solutions. We find the following method yields results that are accurate within 20% for a wide range of parameters. Use Eq. (100), expand H^{nes} to second order in δr_m^{nes} , use $(1 + ax) \approx (1 + x)^a$ for small x and $1 - x^a \approx -a \ln x$ for small a . This gives an approximate relation

$$\frac{\delta r_m^{\text{nes}}}{r_s} \approx 0.17 \alpha_{-1}^{-4/17} M_7^{1/17} f_{-2}^{5/17} q_{-3}^{10/17} r_{s2}^{-5/34} \times \left(\frac{5}{26} \ln \frac{\delta r_m^{\text{nes}}}{\delta r_i} \right)^{4/17}, \quad (110)$$

where $\delta r_i \equiv r_i - r_s$. Eq. (110) can be solved analytically using the Lambert W-function (Corless et al. 1996)¹⁹

$$\mathcal{W}_{-1}(-a) \approx \ln(a) - \ln(-\ln(a)) \quad (111)$$

as

$$\delta r_m^{\text{nes}} = \delta r_i \left[\frac{\mathcal{W}_{-1}(-a)}{-a} \right]^{4/17} = \delta r_i \exp \left[-\frac{4}{17} \mathcal{W}_{-1}(-a) \right], \quad (112)$$

¹⁸ Note that in this section we use $\delta r \equiv r - r_s$ instead of Δ since in this region $\Delta = \max(\delta r, H) = H$ (see Eq. 6).

¹⁹ The Lambert W-function is defined to be the inverse of the function $f(W) = W \exp(W)$, where we need the real branch with the larger absolute value, \mathcal{W}_{-1} , defined on $f > -e^{-1} = -0.368$. The approximation in Eq. (111) is correct to within 20% for all $0 < a < 1/e$.

where the two forms are equivalent, and we have introduced

$$a = 0.465 \alpha_{-1} M_7^{-1/4} f_{-2}^{-5/4} q_{-3}^{-13/12} r_{s2}^{5/8} \left(\frac{\delta r_i}{r_H} \right)^{17/4}. \quad (113)$$

Finally, we substitute in Eq. (102) and use Eq. (101),

$$T_\nu^{\text{nes}}(r_m^{\text{nes}}) = 6.9 \times 10^{47} \text{erg} \alpha_{-1}^{-2/11} M_7^{45/22} f_{-2}^{5/22} q_{-3}^{5/11} r_{s2}^{61/44} \times [-\mathcal{W}_{-1}(-a)]^{13/11}. \quad (114)$$

Note that $\mathcal{W}_{-1}(-a)$ depends logarithmically weakly on the disk parameters (Corless et al. 1996), in practice $1 \leq |\mathcal{W}_{-1}(-a)| \lesssim 10$ for $10^{-4} \lesssim a \leq 1/e = 0.368$. Here $a \leq 1/e$ is required for this solution to exist, implying that q and r_s have to be sufficiently large and small, respectively. In the opposite case, the torque is unsaturated (§ 4.2.2).

4.3 Transition between near and middle zones

4.3.1 The case with overflow

The value of T_ν at the outer edge of the near zone, is to be matched with that in the middle zone, T_{bc} . If the tidal torque is unsaturated in the near zone, we approximate T_{bc} with the asymptotic maximum value, $T_{\text{bc}} = T_{\nu \text{max}}^{\text{neu}}$. Otherwise, if it is saturated, then we set $T_{\text{bc}} = T_\nu^{\text{nes}}(r_m^{\text{nes}})$. Matching the middle and near zones at r_m^{nes} assumes that T_ν does not grow substantially in the transition region between the saturated near zone and the middle zone, i.e. outside of r_m^{nes} but within a radius where the tidal effects are still non-negligible. We find this approximation to be better than 10%. Thus, to match the torque at the outer boundary of the near zone and the inner boundary of the overflowing middle zone, we combine the saturated and unsaturated cases as

$$T_{\text{bc}}^{\text{mo}} = \begin{cases} \min\{T_\nu^{\text{nes}}(r_m^{\text{nes}}), T_{\nu \text{max}}^{\text{neu}}\} & \text{if } a \leq 0.368, \\ T_{\nu \text{max}}^{\text{neu}} & \text{if } a \geq 0.368, \end{cases} \quad (115)$$

where $T_\nu^{\text{nes}}(r_m^{\text{nes}})$ and $T_{\nu \text{max}}^{\text{neu}}$ are given by Eqs. (86) and (114). If this satisfies $T_{\text{bc}}^{\text{mo}} < T_{\text{bc}}^{\text{mg}}$ for $\delta r_i = r_H$ (see Eq. 51), then the satellite migration velocity is less than the gas bulk local inflow velocity, and the overflowing steady-state solution is self-consistent. In the opposite case the disk forms a gap with $\delta r_i > r_H$.

The dimensionless angular momentum flux in the middle zone (Eq. 41) is

$$k_s^{\text{mou}} = 1.3 \alpha_{-1}^{-2} \dot{m}_{-1} M_7^{1/2} f_{-2}^{5/2} q_{-3}^{5/2} r_{s2}^{-1/4} \left[1 + \left(\frac{q}{3} \right)^{1/3} \right]^{-15/2}, \quad (116)$$

$$k_s^{\text{mos}} = 0.97 \alpha_{-1}^{-2/11} \dot{m}_{-1} M_7^{1/22} f_{-2}^{5/22} q_{-3}^{5/11} r_{s2}^{39/44} |\mathcal{W}(a)|^{13/11}. \quad (117)$$

Gap overflow causes the torque level to decrease in the middle zone, which suppresses k . We discuss gap closing in § 4.4 below.

The disk flux in the near zone is larger, due to tidal heating, than in the middle zone. To show this, we next compare the luminosity of the near zone to the middle zone explicitly. In the case of unsaturated torques in the near zone, we find that the local disk luminosity, $L^{\text{neu}}(r) \equiv 4\pi r^2 F^{\text{neu}}$ (see discussion following Eq. 91), peaks sharply near $r_{\text{peak}}^{\text{neu}} = r_s + 1.5 r_H$. We find that the integrated flux from within a ring of width $0.5 r_H$ is approximately

$$k_s^{\text{neu}} = 1.0 \frac{r_H}{r_s} k_s^{\text{mou}}. \quad (118)$$

In the unsaturated case, $r_H/r_s = (q/3)^{1/3} \ll 1$, and so the net luminosity of the middle zone exceeds that of the near zone. For saturated torques, the maximum brightness corresponds to the outer boundary of the near zone, r_m^{nes} . We assume an effective radial width δr_m^{nes} given by Eq. (110). From Eqs. (16) and (109), assuming a radiation pressure dominated near zone, the dimensionless angular momentum flux of the near zone relative to the unperturbed disk is

$$k_s^{\text{nes}} \equiv \frac{4\pi r_m^{\text{nes}} \delta r_m^{\text{nes}} F_m^{\text{nes}}(r_m^{\text{nes}})}{4\pi (r_m^{\text{nes}})^2 F_0(r_1)} = \frac{\delta r_m^{\text{nes}}}{r_m^{\text{nes}}} \frac{H^{\text{nes}}(r_m^{\text{nes}})}{H_0} = \frac{(\delta r_m^{\text{nes}})^2}{r_m^{\text{nes}} H_0} \quad (119)$$

$$= 0.45 \alpha_{-1}^{-8/17} \dot{m}_{-1}^{-1} f_{-2}^{10/17} M_7^{2/17} q_{-3}^{20/17} r_{s2}^{12/17} [-\mathcal{W}(a)]^{8/17}.$$

Comparing Eqs. (117) and (119), and recalling that typically $1 \leq |\mathcal{W}(-a)| \lesssim 10$, we conclude that the luminosity of the saturated near zone can exceed that of the middle zone by a factor between $\sim 3 - 10$ for $q \sim 0.1$.

Given the dimensionless angular momentum flux in the middle zone, the disk parameters and the migration rate are given by Eqs. (43–48). We substitute Eqs. (116–117) to obtain an explicit formula for the disk parameters. The migration rate in the overflowing disk with saturated and unsaturated torques is, respectively,

$$v_{\text{sr}}^{\text{ou}} = 30 \frac{\text{cm}}{\text{s}} \alpha_{-1}^{-2} f_{-2}^{5/2} q_{-3}^{3/2} M_7^{3/2} r_{s2}^{3/4} \left[1 + \left(\frac{q}{3} \right)^{1/3} \right]^{-115/24}, \quad (120)$$

$$v_{\text{sr}}^{\text{os}} = 23 \frac{\text{cm}}{\text{s}} \alpha_{-1}^{-2/11} f_{-2}^{5/22} q_{-3}^{-6/11} M_7^{23/22} r_{s2}^{83/44} [-\mathcal{W}(a)]^{13/11}. \quad (121)$$

4.3.2 Disk with a cavity

Let us next turn to the case with a gap. We determine the radial distance to the outer edge of the gap, λr_s , here by requiring that the migration velocity matches the rescaled gas inflow velocity in the middle zone as stated in the boundary condition, Eq. (13). With λ in hand, Eq. (53–57) determine the disk parameters in the middle zone. The solution is different when the tidal torque is unsaturated near the inner edge and when it is saturated, which we discuss in turn below.

First, assume that the torque is unsaturated all the way outside of the gap ($H \leq r - r_s$). We use Eq. (87) to obtain $\zeta(\lambda r_s, r_s, r_i)$ at the interface between the near and the middle zone. We substitute in (92) to obtain the gas velocity at the interface rescaled by $1/\lambda$:

$$\frac{v_r^{\text{neu}}(\lambda r_s)}{\lambda} = 30 \frac{\text{cm}}{\text{s}} f_{-2} q_{-3}^2 r_{s3}^{-1/2} \lambda^{-3/2} (\lambda - 1)^{-4}. \quad (122)$$

To obtain the migration velocity, we identify $T_{\text{bc}} = T_\nu^{\text{neu}}(\lambda r_s)$ in Eq. (48), and substitute Eq. (80), and eliminate ζ using Eq. (87). This gives

$$v_{\text{sr}} = 8022 \frac{\text{cm}}{\text{s}} \alpha_{-1} \dot{m}_{-1}^{3/2} M_7^{3/4} f_{-2}^{-5/4} q_{-3}^{-7/2} r_{s2}^{9/8} \lambda^{11/16} (\lambda - 1)^{21/4}. \quad (123)$$

The boundary condition, Eq. (13), states that Eqs. (122) and (123) must be equal. This provides a nonlinear equation for λ . We solve this equation perturbatively. To first beyond leading order,

$$\lambda_u = 1 + \delta_u (1 + \delta_u)^{-35/148}, \quad (124)$$

where

$$\delta_u = 0.55 \alpha_{-1}^{-4/37} \dot{m}_{-1}^{-6/37} f_{-2}^{9/37} q_{-3}^{22/37} M_7^{-3/37} r_{s2}^{-13/74}. \quad (125)$$

The ‘u’ subscript is introduced to distinguish the case with unsaturated torques.

Next, consider the case of the torque cutoff. The formulas in § 4.2.3 are not limited to the overflowing case, as long as the torque is saturated ($\delta r \equiv r - r_s \leq H$). If a gap opens then δr_i marks the distance to the edge of the disk in Eq. (98–99), for which $\delta r_i > r_H$. Here, δr_i can be eliminated using the boundary condition Eq. (13) as follows. We identify $\lambda = r_m^{\text{nes}}/r_s$ in Eq. (13) where r_m^{nes} marks the edge of the near zone according to Eq. (109), so that $\lambda = 1 + \delta_1$ where $\delta_1 = \delta r_m^{\text{nes}}/r_s$. Combine Eqs. (107–109) to eliminate $\psi(r_1)$ from the bulk gas velocity at r_1

$$\frac{v_r^{\text{nes}}(r_m^{\text{nes}})}{\lambda} = 0.15 \frac{\text{cm}}{\text{s}} \dot{m}_{-1} f_{-2} q_{-3}^2 r_{s2}^{-3/2} \frac{[1 - (1 + \delta_1)^{-3/2}]}{\delta_1^5}. \quad (126)$$

Similarly, assuming $T_{\text{bc}} = T_\nu^{\text{nes}}(r_m^{\text{nes}})$ in Eq. (48), eliminate $\psi(r_m^{\text{nes}})$ from Eqs. (102) and (109), we get

$$v_{\text{sr}} = 2.0 \times 10^7 \frac{\text{cm}}{\text{s}} \alpha_{-1} f_{-2}^{-5/4} q_{-3}^{-7/2} r_{s2}^{21/8} \frac{(1 + \delta_1)^{-5/4} \delta_1^{13/2}}{[1 - (1 + \delta_1)^{-3/2}]^{5/4}}. \quad (127)$$

The boundary condition, Eq. (13), states that Eqs. (126) and (127) are equal. After rearranging, we get

$$\delta_1 = 0.13 \alpha_{-1}^{-4/37} \dot{m}_{-1}^{4/37} f_{-2}^{9/37} q_{-3}^{22/37} M_7^{-3/37} r_{s2}^{-33/74} \times \left[\frac{3 + 3\delta_1 + \delta_1^2}{1 + (1 + \delta_1)^{3/2}} \right]^{9/37} (1 + \delta_1)^{-17/74}. \quad (128)$$

The last two terms can be omitted within 10% accuracy for $0 < \delta < 3$. This gives the characteristic gap scale in the torque cutoff zone

$$\lambda_s = 1 + 0.13 \alpha_{-1}^{-4/37} \dot{m}_{-1}^{4/37} M_7^{-3/37} f_{-2}^{9/37} q_{-3}^{22/37} r_{s2}^{-33/74}, \quad (129)$$

provided that $\lambda_s - 1 > r_H/r_s$ (i.e. $r - r_s > r_s + r_H$); otherwise no gap is possible.

Thus, the dimensionless angular momentum flux follows after substituting into Eq. (52). In the unsaturated and saturated cases,

$$k_s^{\text{mgu}} = 23 \alpha_{-1}^{1/2} \dot{m}_{0.1}^{-3/8} M_7^{-3/4} q_{-3}^{5/8} \lambda_u^{-11/16} r_{s2}^{-7/8}, \quad (130)$$

$$k_s^{\text{mgs}} = 23 \alpha_{-1}^{1/2} \dot{m}_{0.1}^{-3/8} M_7^{-3/4} q_{-3}^{5/8} \lambda_s^{-11/16} r_{s2}^{-7/8}. \quad (131)$$

The migration speed of the secondary in case of a gap with unsaturated and saturated tidal torques, respectively, is

$$v_{\text{sr}}^{\text{gu}} = -550 \frac{\text{cm}}{\text{s}} \alpha_{-1}^{1/2} \dot{m}_{-1}^{5/8} M_7^{1/4} q_{-3}^{-3/8} \lambda_u^{-11/16} r_{s2}^{1/8}, \quad (132)$$

$$v_{\text{sr}}^{\text{gs}} = -550 \frac{\text{cm}}{\text{s}} \alpha_{-1}^{1/2} \dot{m}_{-1}^{5/8} M_7^{1/4} q_{-3}^{-3/8} \lambda_s^{-11/16} r_{s2}^{1/8}. \quad (133)$$

These estimates depend on the somewhat arbitrary definition of λ that we have adopted in the two cases. In the unsaturated case, we have identified it with the outer edge of the transition region between the near and middle zones, where $\partial_r T_\nu = \dot{M} \partial_r (r^2 \Omega)$, while in the saturated case, we considered it to be the inner edge of the transition region, where $H = r - r_s$. While these conventions could be modified, they do not affect the overflowing solution. They do, however, influence the secondary orbital radius where the gap closes, which we discuss next.

4.4 Gap opening and closing

The previous sections define the disk uniquely, which constitute the solution to the basic equations of § 2. By looking at the solution, we can identify cases where a cavity is kept empty in steady-state or when the disk overflows.

The cavity refills if the inner edge of the disk outside the secondary, r_i , falls within the Hill radius of the secondary. The viscous torque in the near zone, either T_v^{nes} or T_v^{neu} , is a monotonically decreasing function of r_i . Thus, if the disk is truncated, then the viscous torque at any radius in the near zone is decreased relative to its value for an overflowing disk, $r_i = r_s + r_H$ (Eq. 82). This shows that the state of the disk is uniquely determined by the smallest torque barrier²⁰, T_{bc} , or equivalently, the smallest dimensionless angular momentum flux:

$$k_s = \min\{k_s^{\text{mou}}, k_s^{\text{mos}}, k_s^{\text{mgu}}, k_s^{\text{mgs}}\}. \quad (134)$$

given by Eqs. (116–117) and (130–131). We therefore must distinguish four different possible cases of migration and disk behavior. First, $k_s = k_s^{\text{mgu}}$ corresponds to the standard case with a wide gap, with the secondary exhibiting Type-II migration. If $k_s = k_s^{\text{mgs}}$, then the gap edge is located within a scale-height in the near zone so that the torque cutoff limits the tidal torques, but they can nevertheless support a gap against viscosity as the secondary migrates inward. However, if $k_s = k_s^{\text{mos}}$, then the saturated tidal torque becomes smaller than the viscous torque all the way to the Hill radius, and the cavity refills. Finally, if $k_s = k_s^{\text{mou}}$, then the disk reaches the Hill radius and overflows already while the torques in the near zone are still unsaturated.

The migration rate of the secondary is proportional to k_s , (Eq. 48), i.e.

$$|v_{\text{sr}}| = 2k_s \dot{M} r_s / m_s = \min\{v_{\text{sr}}^{\text{ou}}, v_{\text{sr}}^{\text{os}}, v_{\text{sr}}^{\text{gu}}, v_{\text{sr}}^{\text{gs}}\}. \quad (135)$$

given by Eqs. (120–121) and (132–133). Note that $v_{\text{sr}}^{\text{gu}}$ and $v_{\text{sr}}^{\text{gs}}$ are given by practically the same formula, up to an order-of-unity factor of λ . This corresponds to the case of secondary-dominated Type-II migration (Syer & Clarke 1995). The migration rate in the overflowing case is $v_{\text{sr}}^{\text{ou}}$ or $v_{\text{sr}}^{\text{os}}$ for unsaturated or saturated torques. Here the disk is still strongly perturbed, but gas inflow across the orbit limits the efficiency of migration. The disk structure in this new regime is intermediate between a disk with an empty gap (normally associated with Type-II migration) and a weakly perturbed disk (Type-I migration). Although the migration speed in this regime is slower than either in standard Type-II or Type-I migration, we refer to this regime as “Type-1.5”.

The gap can also close due to three dimensional overflow for large secondary masses if the tidal heating is substantial to make the disk puff up. Eq. (56) shows that this happens ($H \gtrsim r$) in a radiation pressure dominated disk if

$$r_s \lesssim r_s^{\text{thick}} = 57 M_\bullet \alpha_{-1}^{4/15} \dot{m}_{-1}^{1/3} M_7^{-2/5} \lambda^{-7/6} q_{-3}^{1/3} \quad (136)$$

or equivalently if

$$q \gtrsim q_{\text{thick}} = 5.4 \times 10^{-3} \alpha_{-1}^{-4/5} \dot{m}_{-1}^{-1} M_7^{6/5} \lambda^{7/2} r_{s2}^3. \quad (137)$$

In this case, we do not derive the geometrically thick overflowing disk or the migration rate.

²⁰ recall that $T_{bc} = T_v$ at the interface between the near and middle zone

We discuss the gap opening and closing conditions in more detail in Paper II, where we contrast them explicitly with the standard expressions widely used in the literature, and also compare Type-1.5 migration to the previously known Type-I and II cases.

5 RESULTS AND DISCUSSION

We have derived analytical solutions to the disk model in different radial regions, where either the tidal, the viscous torques, or the angular momentum flux is negligible relative to the other two terms in Eq. (11). In particular, we have identified the *far zones*, either well inside or outside the secondary’s orbit, where the effects of the secondary are negligible, the exterior *middle zone*, where the disk structure is greatly modified but where the tidal torque and heating are locally negligible, and the *near zones* just inside or outside the secondary, where the tidal effects dominate²¹. We distinguish two cases in the middle zone, depending on whether the disk has a gap (i.e. the disk is truncated well outside the Hill radius) or if the disk is overflowing across the secondary’s orbit. We also distinguish two cases in the near zone outside the secondary’s orbit, depending on whether the tidal torque from the binary is saturated (i.e. whether the location of the cavity edge falls within a scale height H from the secondary). Furthermore, we have investigated asymptotic results for gas and radiation pressure dominated cases.

Distinguishing all of the above cases allowed us to adopt separate approximations, each valid in the corresponding regime, and to derive analytical results to the perturbed accretion disk interacting with the secondary. We further used this to estimate the migration speed for the secondary.

In this section, we collect all of the resulting analytical solutions for the most important disk parameters in the various zones, and present them in a form suitable for easy use. We refer the reader to Paper II for physical interpretations, and discussions on possible implications of our results for real binary systems.

5.1 Disk model

Our results in this paper apply to geometrically thin, optically thick accretion disks, and describe vertically and azimuthally averaged properties. All physical parameters can be written as

$$X(r, r_s, \mathbf{p}) = C \alpha_{-1}^{c_1} \dot{m}_{-1}^{c_2} M_7^{c_3} r_2^{c_4} f_{-2}^{c_5} q_{-3}^{c_6} r_{s2}^{c_7} \Phi(r, r_s, \mathbf{p}) \quad (138)$$

where X denotes any of $\{\Sigma, T_c, H, v_r, F, T_v\}$; r_2 and r_{s2} denote the radius from the primary and the orbital radius of the secondary in units $100 M_\bullet$, respectively; and $\Phi(r, r_s, \mathbf{p})$ denotes an extra function of the parameters $\mathbf{p} = (\alpha, \dot{m}, f, M, q)$. Note that (α, \dot{m}, M) are the usual parameters of a standard solitary accretion disk; q and f represent the mass ratio and the normalization of the azimuthally averaged tidal torque (see Eq. 5). The $_{-N}$ index denotes

²¹ We have further restricted the near zones to lie outside the Hill radius of the secondary.

		cgs value	$[\alpha_{-1}]$	$[\dot{m}_{-1}]$	$[M_7]$	$[r_2]$	$[f_{-2}]$	$[q_{-3}]$	$[r_{s2}]$	Φ
Far zone	Σ_0	4.7(+5)	-4/5	3/5	1/5	-3/5	0	0	0	$\varphi^{3/5}$
Middle with gap	Σ^{mg}	3.6(+6)	-1/2	3/8	-1/4	-9/10	0	3/8	-9/40	$\lambda^{-33/80}$
Middle w/o gap sat.	Σ^{mos}	4.6(+5)	-10/11	0	5/22	-9/10	3/22	3/11	183/220	$ \mathcal{W} ^{13/11}$
Middle w/o gap uns.	Σ^{mou}	5.5(+5)	-2	0	1/2	-9/10	3/2	3/2	3/20	$(\delta r_i/r_H)^{-9/2}$
Near ext. sat.	Σ^{nes}	2.6(+6)	-10/11	0	5/22	-27/26	3/22	3/11	-3/44	$\delta\Omega^{-1/26}\psi^{10/11}$
Near ext. uns.	Σ^{neu}	1.0(+7)	-2	0	1/2	-23/24	3/2	4/3	5/24	$(\delta r/r_s)^{1/2}\zeta_R^2$
Near int.	Σ^{ni}	5.7(+7)	0	1	0	-1/2	-1	-2	0	$ \delta r/r ^4$
Far zone	T_{c0}	5.4(+5)	-1/5	2/5	-1/5	-9/10	0	0	0	$\varphi^{2/5}$
Middle with gap	T_c^{mg}	1.9(+6)	0	1/4	-1/2	-11/10	0	1/4	-3/20	$\lambda^{-11/40}$
Middle w/o gap sat.	T_c^{mos}	5.3(+5)	-3/11	0	-2/11	-11/10	1/11	2/11	61/110	$ \mathcal{W} ^{-26/55}$
Middle w/o gap uns.	T_c^{mou}	6.0(+5)	-1	0	0	-11/10	1	1	1/10	$(\delta r_i/r_H)^{-3}$
Near ext. sat.	T_c^{nes}	1.6(+6)	-3/11	0	-2/11	-25/26	1/11	2/11	-6/11	$\delta\Omega^{1/26}\psi^{3/11}$
Near ext. uns.	T_c^{neu}	6.3(+5)	-1	0	0	-25/24	1	7/6	1/24	$(\delta r/r_s)^{-1/2}\zeta_R$
Near int.	T_c^{ni}	1.5(+6)	0	1/2	-1/4	-9/16	-1/4	-1/2	-5/16	$ \delta r/r ^{5/4}$
Far zone	F_0	7.9(13)	0	1	-1	-3	0	0	0	φ
Middle with gap	F^{mg}	1.8(15)	1/2	5/8	-7/4	-7/2	0	5/8	-3/8	$\lambda^{-11/16}$
Middle w/o gap sat.	F^{mos}	7.6(13)	-2/11	0	-21/22	-7/2	5/22	5/11	61/44	$ \mathcal{W} ^{13/11}$
Middle w/o gap uns.	F^{mou}	1.0(14)	-2	0	-1/2	-7/2	5/2	5/2	1/4	$(\delta r_i/r_H)^{-15/2}$
Near ext. sat.	F^{nes}	9.8(14)	-2/11	0	-21/22	-73/26	5/22	5/11	-93/44	$\delta\Omega^{5/26}\psi^{2/11}$
Near ext. uns.	F^{neu}	6.8(12)	-2	0	-1/2	-77/24	5/2	10/3	-1/24	$(\delta r/r_s)^{-5/2}\zeta_R^2$
Near int.	F^{ni}	3.9(13)	0	1	-1	-7/4	0	0	-5/4	$ \delta r/r $
Far zone	$ v_{r0} $	3.6(+3)	-4/5	3/5	1/5	-2/5	0	0	0	$\varphi^{-3/5}$
Middle with gap	$ v_r^{\text{mg}} $	5.5(+2)	1/2	5/8	1/4	-1/10	0	-3/8	9/40	$\lambda^{33/80}$
Middle w/o gap sat.	$ v_r^{\text{mos}} $	3.7(+3)	9/22	1	-5/22	-1/10	-3/22	-3/11	183/220	$ \mathcal{W} ^{-39/55}$
Middle w/o gap uns.	$ v_r^{\text{mou}} $	3.1(+3)	2	1	-1/2	-1/10	-3/2	-3/2	-3/20	$(\delta r_i/r_H)^{9/2}$
Near ext. sat.	$ v_r^{\text{nes}} $	6.6(+2)	10/11	1	-5/22	1/26	-3/22	-3/11	-41/44	$\delta\Omega^{1/26}\psi^{-10/11}$
Near ext. uns.	$ v_r^{\text{neu}} $	1.7(+2)	2	1	-1/2	-1/24	-3/2	-4/3	-5/24	$(\delta r/r_s)^{-1/2}\zeta_R^{-2}$
Near int.	$ v_r^{\text{ni}} $	3.0(+1)	0	0	0	-1/2	1	2	0	$ \delta r/r ^{-4}$
Far zone	H_0^{rad}	1.5*	0	1	0	0	0	0	0	φ
Middle with gap	$H_{\text{rad}}^{\text{mg}}$	35*	1/2	5/8	-3/4	-1/2	0	1/8	-3/8	$\lambda^{-11/16}$
Middle w/o gap sat.	$H_{\text{rad}}^{\text{mos}}$	1.5*	-2/11	0	1/22	-1/2	5/22	5/11	61/44	$ \mathcal{W} ^{13/11}$
Middle w/o gap uns.	$H_{\text{rad}}^{\text{mou}}$	1.9*	-2	0	1/2	-1/2	5/2	5/2	1/4	$(\delta r_i/r_H)^{-15/2}$
Near ext. sat.	$H_{\text{rad}}^{\text{nes}}$	19*	-2/11	0	1/22	5/26	5/22	5/11	39/44	$\delta\Omega^{5/26}\psi^{2/11}$
Near ext. uns.	$H_{\text{rad}}^{\text{neu}}$	0.13*	-2	0	1/2	-5/24	5/2	10/3	-1/24	$(\delta r/r_s)^{-5/2}\zeta_R^2$
Near int.	$H_{\text{rad}}^{\text{ni}}$	0.75*	0	1	0	0	0	0	0	$ \delta r/r $
Far zone	H_0^{gas}	0.28*	-1/10	1/5	-1/10	21/20	0	0	0	$\varphi^{1/5}$
Middle with gap	$H_{\text{gas}}^{\text{mg}}$	0.53*	0	1/8	-1/4	19/20	0	1/8	-3/40	$\lambda^{-11/16}$
Middle w/o gap uns.	$H_{\text{gas}}^{\text{mou}}$	0.29*	-1/2	0	0	19/20	1/2	1/2	1/20	$(\delta r_i/r_H)^{-3/2}$
Near ext. uns.	$H_{\text{gas}}^{\text{neu}}$	0.23*	-1/2	0	0	47/48	1/2	7/12	1/48	$(\delta r/r_s)^{-1/4}\zeta_R^{1/2}$
Near int.	$H_{\text{gas}}^{\text{ni}}$	0.36*	0	1/4	-1/8	29/32	-1/8	-1/4	-5/32	$ \delta r/r ^{5/8}$
Far zone	$T_{\nu 0}$	7.1(47)	0	1	2	1/2	0	0	0	φ
Middle with gap	T_{ν}^{mg}	1.6(49)	1/2	5/8	5/4	0	0	5/8	-3/8	$\lambda^{-11/6}$
Middle w/o gap sat.	T_{ν}^{mos}	6.9(47)	-2/11	0	45/22	0	5/22	5/11	61/44	$ \mathcal{W} ^{13/11}$
Middle w/o gap uns.	T_{ν}^{mou}	9.1(47)	-2	0	5/2	0	5/2	5/2	1/4	b^3
Near ext. sat.	T_{ν}^{nes}	1.1(49)	-2/11	0	45/22	0	5/22	5/11	61/44	$\psi^{13/11}$
Near ext. uns.	T_{ν}^{neu}	1.7(49)	-2	0	5/2	0	5/2	5/2	1/4	ζ_R^3
Near int.	T_{ν}^{ni}	2.4(50)	1	3/2	7/4	15/16	-5/4	-5/2	-5/16	$ \delta r/r ^{21/4}$
GW inspiral	$ v_{\text{sr,GW}} $	380	0	0	0	0	0	1	-3	
Type-II	$ v_{\text{sr,II}} $	550	1/2	5/8	1/4	0	0	-3/8	1/8	$\lambda^{-11/16}$
Type-1.5 sat.	$ v_{\text{sr,1.5s}} $	23	-2/11	0	23/22	0	5/22	-6/11	83/44	$ \mathcal{W} ^{13/11}$
Type-1.5 uns.	$ v_{\text{sr,1.5u}} $	31	-2	0	3/2	0	5/2	3/2	3/4	b^3
Middle gap uns.	k_s^{mgu}	23	1/2	-3/8	-3/4	0	0	5/8	-7/8	$\lambda_u^{-11/16}$
Middle gap sat.	k_s^{mgs}	23	1/2	-3/8	-3/4	0	0	5/8	-7/8	$\lambda_s^{-11/16}$
Middle w/o gap uns.	k_s^{mou}	1.3	-2	-1	1/2	0	5/2	5/2	-1/4	b^3
Middle w/o gap sat.	k_s^{mos}	0.97	-2/11	-1	1/22	0	5/22	5/11	39/44	$ \mathcal{W} ^{13/11}$
Near ext. sat.	k_s^{nes}	5.5	-4/17	-1	1/17	0	5/17	10/17	29/34	$ \mathcal{W} ^{4/17}$
argument of \mathcal{W}	$-a$	-0.465	1	0	-1/4	0	-5/4	-13/12	5/8	$(\delta r_i/r_H)^{17/4}$

Table 2. Pre-factors and exponents in the analytical disk model in different zones, C and c_i in Eq. (138). The third column is in cgs units except where marked by * (where it is in units of GM_{\bullet}/c^2). Columns 4–10 are exponents, the last column is the extra multiplicative function (see text). The last two block of parameters show the migration rate of the secondary and other useful parameters.

		C	$[\alpha_{-1}]$	$[\dot{m}_{-1}]$	$[M\tau]$	$[f_{-2}]$	$[q_{-3}]$	$[r_{s2}]$	Φ
Middle/Far w. gap sat.	r_f^{mgs}/r_s	540	1	-3/4	-3/2	0	5/4	-7/4	$(1 + \delta_{\text{mg}}^{\text{nes}})^{-11/8}$
Middle/Far w. gap uns.	r_f^{mgu}/r_s	540	1	-3/4	-3/2	0	5/4	-7/4	$(1 + \delta_{\text{mg}}^{\text{neu}})^{-11/8}$
Near ext./middle w. gap sat.	$\delta_{\text{mg}}^{\text{nes}}$	0.130	-4/37	4/37	-3/37	9/37	22/37	-33/74	
Near ext./middle w. gap uns.	$\delta_{\text{mg}}^{\text{neu}}$	0.55	-4/37	-6/37	-3/37	9/37	22/37	-13/74	$(1 + \delta_{\text{mg}}^{\text{neu}})^{-35/148}$
Near ext./middle w/o gap sat.	$\delta_{\text{mo}}^{\text{nes}}$	0.083	-4/17	0	1/17	5/17	10/17	-5/34	$ \mathcal{W} ^{4/17}$
Near ext./middle w/o gap uns.	$\delta_{\text{mo}}^{\text{neu}}$	0.35	-4/7	-2/7	1/7	5/14	20/21	-1/14	$(r_i/r_s)^{-115/126}$
Far/Near int.	$\delta_{\text{ni}}^{\text{f}}$	-0.1	-4/17	-2/17	1/17	5/17	10/17	-1/34	$(1 + \delta_{\text{ni}}^{\text{f}})^{-841/714}$

Table 3. Transition radii between different zones relative to the secondary orbital radius, r_s . Here r_a^b is the radius at the interface between zone a and b , $\delta r_a^b \equiv r_a^b - r_s$, and $\delta_a^b \equiv \delta r_a^b / r_s$. Different columns show the constant prefactor and exponents in Eq. (138) as in Table 2.

normalizing with 10^{-N} , e.g. $q_{-3} = q/10^{-3}$. The C prefactor, c_i exponents, and the Φ function in Eq. (138) are given in Table 2 in the different zones and cases for β -disks (i.e. $\nu \propto p_{\text{gas}}$). For β -disks, many of the physical parameters, including the surface density, Σ , and the central temperature, T_c , are independent of whether gas or radiation pressure dominates. This, however, is not true for the scale-height, where we quote results in both regimes, labeled with a ‘‘gas’’ or ‘‘rad’’ subscript.

The last column of Table 2 shows $\Phi(r, r_s, \mathbf{p})$ in Eq. (138). Here we introduced the following notation:

$$\delta r = r - r_s, \quad \delta r_i = r_i - r_s, \quad (139)$$

$$\lambda_s = 1 + \delta_{\text{mg}}^{\text{nes}}, \quad \lambda_u = 1 + \delta_{\text{mg}}^{\text{neu}}, \quad (140)$$

$$\delta\Omega \equiv (\Omega_s - \Omega)/\Omega_s = 1 - (r/r_s)^{-3/2}, \quad (141)$$

$$\delta\Omega_0 \equiv (\Omega_s - \Omega_0)/\Omega_s = 1 - (r_i/r_s)^{-3/2}, \quad (142)$$

$$\varphi \equiv 1 - \left(\frac{r_{\text{ISCO}}}{r}\right)^{1/2}, \quad (143)$$

$$\begin{aligned} \zeta_{\text{R}} &\equiv \frac{r_{\text{H}}^{5/2}}{r_s^{5/2}} \int_{r_i/r_s}^{r/r_s} x^{-7/6} \left(1 - x^{-3/2}\right)^{-1/6} (x-1)^{-10/3} dx \\ &\approx \frac{2^{1/6}}{3^{1/6}} \frac{2}{5} \frac{(r_i/r_s)^{-115/72}}{(\delta r_i/r_{\text{H}})^{5/2}} \left[1 - \left(\frac{r_i}{r}\right)^{115/72} \left(\frac{\Delta_i}{\Delta}\right)^{5/2}\right], \end{aligned} \quad (144)$$

$$\begin{aligned} \psi &\equiv \frac{2}{3} \int_{\delta\Omega}^{\delta\Omega_0} x^{-21/26} (1-x)^{-6/13} dx \\ &= \frac{2}{3} B(\delta\Omega; 5/26, 7/13) - \frac{2}{3} B(\delta\Omega_0; 5/26, 7/13) \\ &\approx 0.4 \ln \frac{\delta r}{\delta r_i}, \end{aligned} \quad (145)$$

$$\mathcal{W} \equiv \mathcal{W}_{-1}(-a) \approx \ln(a) - \ln(-\ln(a)), \quad (146)$$

$$b \approx \left(\frac{r_i}{r_s}\right)^{-115/72} \left(\frac{\delta r_i}{r_{\text{H}}}\right)^{-5/2}. \quad (147)$$

Here $B(x; a, b)$ is the incomplete Beta function, and \mathcal{W} is the Lambert-W function, the branch defined on the negative real axis, evaluated at $-a$ given in the last row of Table 2. Typically, $1 \leq |\mathcal{W}(-a)| \lesssim 10$. The approximations shown for ψ and \mathcal{W} are better than 20%. Here, r_{ISCO} is the innermost stable circular orbit near the SMBH (i.e. $6 M_{\bullet}$ ($1 M_{\bullet}$) for a non-spinning (maximally spinning) SMBH), $r_{\text{H}} = (q/3)^{1/3} r_s$ is the Hill radius, r_i marks the radius at which the viscous torque becomes very small outside the secondary’s orbit for which we use

$$\delta r_i = r_{\text{H}} \quad \text{if } k_s = k_s^{\text{mou}} \text{ or } k_s = k_s^{\text{mos}}, \quad (148)$$

and λ is the dimensionless gap or truncation radius scale

$$\lambda = \begin{cases} \lambda_u & \text{if } k_s = k_s^{\text{mgu}}, \\ \lambda_s & \text{if } k_s = k_s^{\text{mgs}}, \end{cases} \quad (149)$$

where²²

$$k_s = \{k_s^{\text{mou}}, k_s^{\text{mos}}, k_s^{\text{mgu}}, k_s^{\text{mgs}}\} \quad (150)$$

is the dimensionless angular momentum flux or *brightening factor*.

We collect the formulae for the transition radii separating different radial zones and physical regimes in Table 3. We label $\delta_a^b = (r_a^b - r_s)/r_s$, where r_a^b marks the radius of the interface between zone a and b . For example, $\delta_{\text{mg}}^{\text{nes}}$ is the transition between the middle zone and the torque-saturated exterior near zone if there is a wide gap, which also sets the truncation radius scale λ_s in Eq. (140).

The state of the disk and the migrate speed of the binary is directly set by the dimensionless angular momentum flux k_s . If $k_s = [k_s^{\text{mou}}]k_s^{\text{mos}}$, then the disk is in the [un]saturated overflowing state, whereas if $k_s = [k_s^{\text{mgu}}]k_s^{\text{mgs}}$ then it is in the [un]saturated state with a wide gap. These four possibilities are indicated in Table 2. The appropriate choice of k_s also determines which case in Table 2 are to be used in the middle zone for the other parameters (‘mou’, ‘mos’, or ‘mg’), and in the near exterior zone (‘neu’ or ‘nes’).

Thus, the ‘‘phase space’’ of solutions consists of four regions²³. The transition between two different solutions, with or without wide gaps, corresponds to the parameters for which $k_s^{\text{mos}} = k_s^{\text{mgs}}$ or $k_s^{\text{mou}} = k_s^{\text{mgu}}$. Our hypothesis is that this must represent a physical transition in the disk+binary system, as the secondary migrates inward from large radius. Initially, a central cavity is created, and the outer edge of the cavity lies far from the secondary’s orbit. However, as the secondary migrates inward, the distance between the cavity edge and the secondary shrinks (at least when measured in units of the Hill radius of the secondary). This may happen both because the viscosity increases as the pressure grows during pile-up, and also because the tidal torque decreases with increasing scaleheight due to the torque cutoff. The cavity finally closes once the cavity wall nudges inside the Hill radius. The dimensionless angular momentum flux or brightening factor, k_s , is largest when this transition occurs.

²² If either k_s^{mgu} , k_s^{mgs} , k_s^{mou} , or k_s^{mos} is less than one, then the disk does not have a middle zone by definition, and the disk is not strongly perturbed.

²³ Here we assume that GW emission is negligible, and the disk drives the binary. See Paper II for further discussion.

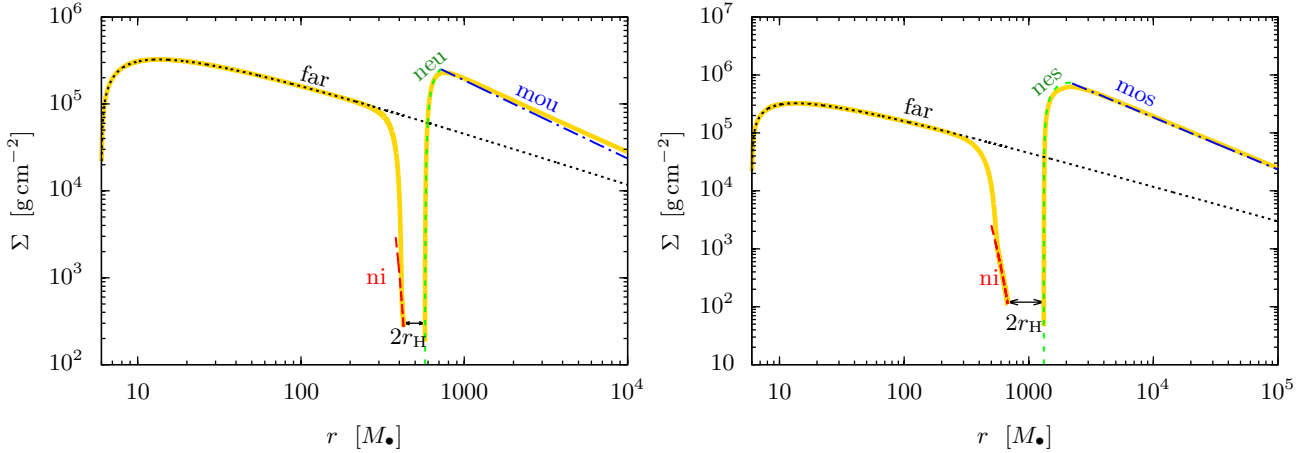


Figure 2. Comparison of the numerical solution (thick yellow solid lines) with the asymptotic analytical approximations in the various zones (dotted, dashed, and dash-dotted lines, labeled as in Table 2) for the surface density of the disk around a $10^5 M_{\odot}$ primary. The mass ratio and binary separation are $(q, r_s) = (0.01, 500 M)$ and $(0.1, 1000 M)$ on the left and right panels, respectively. In both cases the disk is in the overflowing steady-state. The tidal torque is unsaturated in the near zone outside the Hill radius on the left panel, but it is saturated on the right panel. The disk structure is significantly modified in both cases in an extended region around the secondary.

These gap opening/closing conditions are quite different from those in the literature (e.g. Ward 1986), which state that the gap closes if the disk extends into the region closer than either the local scaleheight or the Hill radius from the secondary. Note that our gap closing condition combines statements on the scaleheight and the Hill radius, but since the scaleheight and viscosity vary significantly near the secondary in the strongly perturbed case with a large pile-up, they depend on the actual perturbed profiles rather than the averaged quantities describing accretion disks around a solitary object. We discuss gap opening/closing, and its physical implications, in more detail in Paper II.

We have verified that the analytical approximate solutions to the disk model match the numerical solutions typically to within tens of percent for a wide range of disk and binary parameters when the disk is strongly perturbed. Figure 2 shows two examples when the disk is in the overflowing state with unsaturated (left panel) and saturated (right panel) tidal torques near the secondary. Different regions are indicated with the abbreviations used in Table 2. For further examples and other physical quantities, see Paper II.

5.2 Brightening factor

As stated in the previous sections, the k_s parameter sets the angular momentum flux and the brightness of the disk in the middle zone relative to the unperturbed value, and determines the state of the disk.

Remarkably, the disk parameters can differ dramatically from the unperturbed values not only in the near zone, where the tidal effects dominate, but also in the middle zone, where tidal effects are already negligible. The tidal effects of the secondary are short-range, but the corresponding effect is communicated to distant regions by setting an effective boundary condition. The size of this region can be $r_f^{\text{mg}}/r_s \sim 540 \alpha_{-1} \dot{m}_{-1}^{-3/4} M_7^{-3/2} r_{s2}^{-7/4} q_{-3}^{5/4}$ times larger than the secondary orbital radius (see Table 3). This long-range behavior is confirmed in our full numerical solutions and is also present in Lodato et al. (2009) and Chang et al. (2010)

for a circumbinary disk with a cavity. The same k_s parameter also sets the increase in the scale-height, as well as the migration speed of the secondary. We have derived the analytical formulae for k_s in the four relevant regimes summarized in the previous section. Due to its extended radial size, the integrated luminosity of the middle zone is often larger than that of the near zone in the torque-unsaturated case, overflowing state. However, the near zone may be brighter than the middle zone, when the system is in the torque-saturated, overflowing state (see Paper II for further discussions).

5.3 Migration rate

Finally, we have derived the migration speed of the secondary; approximate analytical formulae for our results are listed in Table 2. We find that in the regimes when a cavity forms, the migration in our solution is slower than the standard steady-state secondary-dominated Type-II migration rate (Syer & Clarke 1995) by a factor $\lambda^{11/16} \sim 2$. The Type-II rate may be further reduced in non-steady state models if the accretion rate or the gas mass is limited (Ivanov et al. 1999; Lodato et al. 2009). However, in the new ‘‘Type-1.5’’ regime we identify, with a partial pile-up and overflow, the migration is even slower.

More generally, the migration speed for a strongly perturbed disk follows the minimum of the three possible solutions:

$$|v_{\text{sr}}| = \min(|v_{\text{sr},1.5\text{s}}|, |v_{\text{sr},1.5\text{u}}|, |v_{\text{sr,II}}|). \quad (151)$$

In general, Type-1.5 migration is more rapid at larger r_s , in contrast with the Type-II rate, which is nearly constant, and the GW inspiral rate, which strongly decreases with r_s . Therefore, as a real system evolves, it will first transition from an initial Type-II migration at large radii to Type-1.5 migration at smaller radii, before finally being driven by GWs at still smaller separations.

Regarding the dependence on the primary mass, the Type-II is nearly constant, while the Type-1.5 speed in-

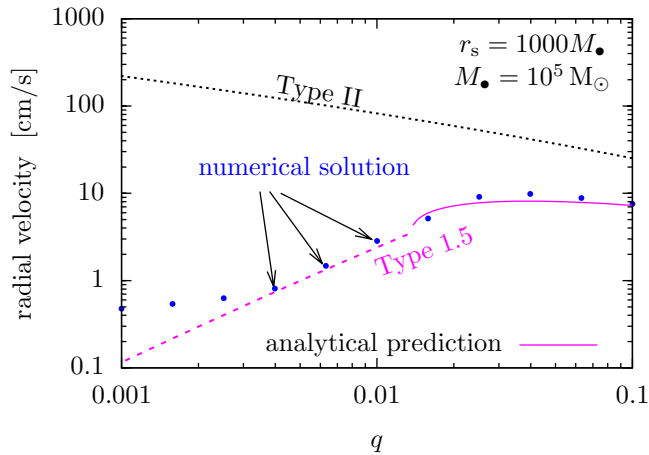


Figure 3. The migration speed of the secondary for different mass ratios for $M_{\bullet} = 10^5 M_{\odot}$ at $r_s = 1000 M_{\bullet}$ (or $t_{\text{orb}} = 1$ day). The steady-state numerical solutions (blue) are well represented by our analytical formula for Type-1.5 migration (magenta), but not by those for Type-I or II (black dotted). The dashed and solid magenta lines show the unsaturated and saturated Type-1.5 cases, respectively. The discrepancy between the numerical and analytical solutions become more significant at $q < 0.002$ due to the fact that the disk is not strongly perturbed there.

creases with M_{\bullet} . This implies that at any fixed orbital separation, Type-1.5 migration is relevant for lower masses (roughly those in the range expected to be detectable by a space-based gravitational wave mission such as *LISA*, and Type-II is relevant for higher-mass binaries (in the sensitivity range of Pulsar Timing Arrays; see Paper II). Type-1.5 migration may also be important for stellar mass binaries in proto-stellar disks or Jupiter-mass planets around M-type dwarf stars of mass (0.1–1) M_{\odot} (see Johnson et al. 2012, for a recent discovery of such a system). Finally, we note that Type-1.5 (Type-II) migration operates for larger (smaller) accretion rates, if fixing all other parameters.

All of the above conclusions are based on the analytical solutions we obtained; however, we have verified, by numerically solving the equations presented in § 2, that our solutions are accurate to within tens of percent for a broad range of parameters. In particular, in Figure 3 we show the analytical approximation of the migration rates for the case of $r_s = 1000 M_{\bullet}$ for $M_{\bullet} = 10^5 M_{\odot}$, together with the rates obtained from a numerical solution. In this case, a disk is in the overflowing state for all values of $q \gtrsim 10^{-3}$ shown, and the migration rate is significantly different from both Type-I and II. As the figure shows, the analytical Type-1.5 formulas give a good approximation over a wide range of q for the migration speed.

5.4 Caveats

Our findings are subject to many possible caveats.

- We assumed a radiatively efficient disk model in which the effective viscosity is proportional to the gas pressure in the disk with a constant α coefficient even in the radiation pressure dominated regime. Future studies should investigate alternative models in which the viscosity is proportional to the total gas+radiation pressure (Shakura & Sunyaev

1973), or where the viscosity is generated by magneto-rotational instability (MRI, see Turner et al. 2003; Shi et al. 2012; Giacomazzo et al. 2012; Noble et al. 2012 for simulations of circumbinary disks leading to an “antigap”).

- We assumed steady-state models where the accretion rate is constant over radius. This is expected to be valid as long as the gas inflow is much faster than the migration rate of the secondary over a large range of radii, if the total gas supply is not limited, and if the accretion rate is set at the inner or outer boundary (i.e. for the new Type-1.5 migration regime we focus on here). However, this assumption may be violated for tidally truncated circumbinary disks (Type-II migration, Ivanov et al. 1999) or for models where the gas supply rate is limited at the outer boundary (Lodato et al. 2009; Rafikov 2012).

- We assumed unequal-mass binaries, averaged over the azimuthal angle, assumed that the density waves generated by secondary are dissipated locally, and that the radial tidal torque profile follows the formula given by Armitage & Natarajan (2002). This assumes that the tidal torque saturates near the secondary at a radial distance closer than the scaleheight ($\partial_r T_d \propto H^{-4}$). We also assumed that the gas entering a distance comparable to the Hill radius can flow freely across the secondary’s orbit. However, accretion onto the secondary may affect the Type-1.5 migration rate. Farther away from the secondary, the assumed torque density has a steep cutoff ($\partial_r T_d \propto |r - r_s|^{-4}$); extrapolating beyond $r > 2r_s$ might be inaccurate. The $|r - r_s|^{-4}$ scaling may also be inaccurate in the local nonlinearly perturbed regime especially for comparable mass-ratio binaries (MacFadyen & Milosavljević 2008; Roedig et al. 2012; Petrovich & Rafikov 2012). These issues should be investigated using simulations, which could also address comparable mass binaries where the disk may be significantly non-axisymmetric (e.g. MacFadyen & Milosavljević 2008; Cuadra et al. 2009) and where the accretion of the secondary is non-negligible (Lubow et al. 1999).

- We neglected non-axisymmetric inflow into the secondary’s orbit or onto the secondary if a cavity is formed. Inflow across the gap or accretion of the secondary reduces the amount of pile up outside the secondary, reduces the Type-II migration rate, and could affect the gap closing transition between the continuously overflowing solutions and the cases with a gap. We have also neglected the corotation torques in the overflowing case.

- We found that the enhanced pressure dominates over the increase in surface density outside the secondary’s orbit, which makes the overflowing disk stable against gravitational fragmentation (see Paper II). However, the steep pressure gradient in the near zone around a massive secondary may lead to global non-axisymmetric dynamical instabilities (Papaloizou & Pringle 1985; Goldreich et al. 1986). The corresponding enhancement of the effective viscosity and angular momentum transport in the disk might reduce the pile-up outside the secondary’s orbit and further reduce the Type-1.5 migration rate. A detailed stability analysis and an investigation of its implications goes beyond the scope of this paper.

- We restricted our attention to circular binaries. However, binary eccentricity may be excited in cases with a cavity, when the masses of the two compact objects are comparable and the gap edge itself becomes significantly non-

axisymmetric (Artymowicz 1992; Armitage & Natarajan 2005; Roedig et al. 2011, 2012). We note that such non-axisymmetries excited in disks with a gap diminish once the mass ratio is $q \lesssim 0.1$ (D’Orazio et al. 2012, in preparation). Nevertheless, it remains to be seen if the binary develops significant eccentricities in the unequal-mass, overflowing state, with a significant pile-up.

- We assumed that the binary is sufficiently widely separated that gravitational wave emission is negligible. For a complete picture, future studies should investigate the gravitational wave driven regime (Tanaka & Menou 2010; Chang et al. 2010; Yunes et al. 2011; Kocsis et al. 2011; Farris et al. 2011; Tanaka et al. 2012; Bode et al. 2012; Baruteau et al. 2012; Giacomazzo et al. 2012; Noble et al. 2012).

6 CONCLUSIONS

In summary, we have presented new analytical solutions to disk properties and migration rates, obtained from self-consistent solutions of a coupled binary-disk system. The evolution equations are solved analytically in the strongly perturbed limit, including the angular momentum exchange between the disk and the binary and the modifications to the density, scale-height, and viscosity self-consistently, including viscous and tidal heating, diffusion limited cooling, radiation pressure, and the orbital decay of the binary.

In addition to recovering solutions with a central cavity, similar to previous “Type-II migration” scenarios, we have identified a distinct new regime, applicable at smaller separations and masses, larger accretion rates, and mass ratios in the range $10^{-3} \lesssim q \lesssim 0.1$. For these systems, gas piles up outside the binary’s orbit, but rather than creating a cavity, it continuously overflows as in a porous dam. The disk properties are intermediate between those in an unperturbed disk and a disk with a wide gap. The migration rate of the secondary in this “Type 1.5” regime is typically slower than both Type-I and Type-II rates.

In this paper, we have presented simple analytical formulae that comprehensively describe binary systems with different parameters, in various stages of evolution. The analytical results provide simple scaling relations, which may be useful to scale and interpret the results of numerical simulations to different disk or binary parameters. It allows us to map out the effects of varying α , \dot{m} , or the binary parameters, over a wide range from planetary disks to active galactic nuclei around SMBH binaries.

We discuss the applicability of the new Type-1.5 regime and its physical implications for specific systems, as well as possible observable signatures in a companion paper (Kocsis et al. 2012).

ACKNOWLEDGMENTS

We thank Re’em Sari, Taka Tanaka, Alberto Sesana, and Roman Rafikov for useful discussions. BK acknowledges support from NASA through Einstein Postdoctoral Fellowship Award Number PF9-00063 issued by the Chandra X-ray Observatory Center, which is operated by the Smithsonian Astrophysical Observatory for and on behalf of the

National Aeronautics Space Administration under contract NAS8-03060. This work was supported in part by NSF grant AST-0907890 and NASA grants NNX08AL43G and NNA09DB30A (to AL) and NASA grant NNX11AE05G (to ZH).

APPENDIX A: VISCOUSLY AND TIDALLY HEATED DISKS

Here we provide the details of the algebraic manipulations that give the disk model for fixed F and D_ν for either α or β -disks (i.e. $b = 0$ or 1).

For fixed β , we can reduce the problem to 3 equations and 3 unknowns Σ, T, ν . From Eqs. (15), (17), and (18),

$$\Sigma \nu = \frac{8}{9\Omega^2} D_\nu = \alpha \frac{\kappa^2}{\Omega^3} \frac{\beta^b F^2}{(1-\beta)^2} \Sigma \quad (\text{A1})$$

$$F = \frac{8}{3} \frac{\sigma T_c^4}{\kappa \Sigma} \quad (\text{A2})$$

Solve this for Σ and T ,

$$\Sigma = \frac{8c^2}{9\alpha\kappa^2} \Omega \frac{(1-\beta)^2}{\beta^b} \frac{D_\nu}{F^2} \quad (\text{A3})$$

$$T_c^4 = \frac{c^2}{3\alpha\kappa\sigma} \Omega \frac{(1-\beta)^2}{\beta^b} \frac{D_\nu}{F} \quad (\text{A4})$$

Finally β is given by

$$\frac{\beta}{1-\beta} = \frac{p_{\text{gas}}}{p_{\text{rad}}} = \frac{3\rho k T_c}{a\mu m_p T_c^4} = \frac{3k}{a\mu m_p} \frac{\Sigma}{2HT_c^3} \quad (\text{A5})$$

where Σ, T_c , and H are to be substituted from Eqs. (A3), (A4), and (16). From this

$$\frac{\beta^{(1/2)+(b-1)/10}}{1-\beta} = \frac{c[k/(\mu m_p)]^{2/5}}{(3\alpha\sigma)^{1/10}\kappa^{9/10}} \Omega^{9/10} \frac{D_\nu^{1/10}}{F^{9/10}} \quad (\text{A6})$$

Finally Eqs. (A3) and (A4) can be simplified by eliminating $1-\beta$ using Eq. (A6), which leads to Eq. (21–22).

REFERENCES

- Armitage P. J., Natarajan P., 2002, *ApJ*, 567, L9
 Armitage P. J., Natarajan P., 2005, *ApJ*, 634, 921
 Artymowicz P., 1992, *PASP*, 104, 769
 Artymowicz P., 1993a, *ApJ*, 419, 166
 Artymowicz P., 1993b, *ApJ*, 419, 155
 Baruteau C., Ramirez-Ruiz E., Masset F., 2012, *MNRAS*, p. L436
 Bate M. R., Lubow S. H., Ogilvie G. I., Miller K. A., 2003, *MNRAS*, 341, 213
 Blaes O., Krolik J. H., Hirose S., Shabaltas N., 2011, *ApJ*, 733, 110
 Bode T., Bogdanović T., Haas R., Healy J., Laguna P., Shoemaker D., 2012, *ApJ*, 744, 45
 Chang P., Strubbe L. E., Menou K., Quataert E., 2010, *MNRAS*, 407, 2007
 Corless R., Gonnet G., Hare D., Jeffrey D., Knuth D., 1996, *Advances in Computational Mathematics*, 5, 329
 Crida A., Morbidelli A., 2007, *MNRAS*, 377, 1324
 Cuadra J., Armitage P. J., Alexander R. D., Begelman M. C., 2009, *MNRAS*, 393, 1423
 D’Angelo G., Henning T., Kley W., 2003, *ApJ*, 599, 548

- Dong R., Rafikov R. R., Stone J. M., 2011, *ApJ*, 741, 57
- Dong R., Rafikov R. R., Stone J. M., Petrovich C., 2011, *ApJ*, 741, 56
- Duffell P. C., MacFadyen A. I., 2012, *ApJ*, submitted, e-print arXiv:1202.5608
- Farris B. D., Liu Y. T., Shapiro S. L., 2011, *Phys. Rev. D*, 84, 024024
- Frank J., King A., Raine D. J., 2002, *Accretion Power in Astrophysics: Third Edition*
- Giacomazzo B., Baker J. G., Miller M. C., Reynolds C. S., van Meter J. R., 2012, e-prints arXiv:1203.6108
- Goldreich P., Goodman J., Narayan R., 1986, *MNRAS*, 221, 339
- Goldreich P., Tremaine S., 1980, *ApJ*, 241, 425
- Goldreich P., Tremaine S., 1982, *ARA&A*, 20, 249
- Goodman J., 2003, *MNRAS*, 339, 937
- Goodman J., Rafikov R. R., 2001, *ApJ*, 552, 793
- Goodman J., Tan J. C., 2004, *ApJ*, 608, 108
- Haiman Z., Kocsis B., Menou K., Lippai Z., Frei Z., 2009, *Classical and Quantum Gravity*, 26, 094032
- Hirata C. M., 2011a, *MNRAS*, 414, 3198
- Hirata C. M., 2011b, *MNRAS*, 414, 3212
- Hourigan K., Ward W. R., 1984, *Icarus*, 60, 29
- Ivanov P. B., Papaloizou J. C. B., Polnarev A. G., 1999, *MNRAS*, 307, 79
- Johnson J. A., Gazak J. Z., Apps K., Muirhead P. S., Crepp J. R., Crossfield I. J. M., Boyajian T., von Braun K., Rojas-Ayala B., Howard A. W., Covey K. R., Schlawin E., Hamren K., Morton T. D., Marcy G. W., Lloyd J. P., 2012, *AJ*, 143, 111
- Kley W., Crida A., 2008, *A&A*, 487, L9
- Kocsis B., Haiman Z., Loeb A., 2012, *MNRAS*, submitted, e-print arXiv:1202.5268 (Paper II)
- Kocsis B., Yunes N., Loeb A., 2011, *Phys. Rev. D*, 84, 024032
- Korycansky D. G., Papaloizou J. C. B., 1996, *ApJS*, 105, 181
- Lin D. N. C., Papaloizou J., 1986, *ApJ*, 309, 846
- Liu Y. T., Shapiro S. L., 2010, *Phys. Rev. D*, 82, 123011
- Lodato G., Nayakshin S., King A. R., Pringle J. E., 2009, *MNRAS*, 398, 1392
- Lubow S. H., Seibert M., Artymowicz P., 1999, *ApJ*, 526, 1001
- Lynden-Bell D., Pringle J. E., 1974, *MNRAS*, 168, 603
- MacFadyen A. I., Milosavljević M., 2008, *ApJ*, 672, 83
- Meyer-Vernet N., Sicardy B., 1987, *Icarus*, 69, 157
- Noble S. C., Mundim B. C., Nakano H., Krolik J. H., Campanelli M., Zlochower Y., Yunes N., 2012, *ApJ*, submitted, e-print arXiv:1204.1073
- Novikov I. D., Thorne K. S., 1973, in Dewitt C., Dewitt B. S., eds, *Black Holes (Les Astres Occlus) Astrophysics of black holes..* pp 343–450
- Paardekooper S.-J., Mellema G., 2006, *A&A*, 459, L17
- Paardekooper S.-J., Mellema G., 2008, *A&A*, 478, 245
- Papaloizou J. C. B., Pringle J. E., 1985, *MNRAS*, 213, 799
- Penna R. F., McKinney J. C., Narayan R., Tchekhovskoy A., Shafee R., McClintock J. E., 2010, *MNRAS*, 408, 752
- Petrovich C., Rafikov R. R., 2012, *ArXiv e-prints*
- Pringle J. E., 1991, *MNRAS*, 248, 754
- Rafikov R. R., 2012, *ArXiv e-prints*
- Rafikov R. R., Petrovich C., 2012, *ApJ*, 747, 24
- Roedig C., Dotti M., Sesana A., Cuadra J., Colpi M., 2011, *MNRAS*, 415, 3033
- Roedig C., Sesana A., Dotti M., Cuadra J., Amaro-Seoane P., Haardt F., 2012, *MNRAS*, submitted, e-print arXiv:1202.6063
- Sakimoto P. J., Coroniti F. V., 1981, *ApJ*, 247, 19
- Salem M. A., Kocsis B., Haiman Z., 2012, in preparation
- Shakura N. I., Sunyaev R. A., 1973, *Astron. Astroph.*, 24, 337
- Shi J.-M., Krolik J. H., Lubow S. H., Hawley J. F., 2012, *ApJ*, 749, 118
- Syer D., Clarke C. J., 1995, *MNRAS*, 277, 758
- Tanaka T., 2011, *MNRAS*, 410, 1007
- Tanaka T., Menou K., 2010, *ApJ*, 714, 404
- Tanaka T., Menou K., Haiman Z., 2012, *MNRAS*, 420, 705
- Turner N. J., Stone J. M., Krolik J. H., Sano T., 2003, *ApJ*, 593, 992
- Ward W. R., 1986, *Icarus*, 67, 164
- Ward W. R., 1997, *Icarus*, 126, 261
- Ward W. R., Hourigan K., 1989, *ApJ*, 347, 490
- Yunes N., Kocsis B., Loeb A., Haiman Z., 2011, *Physical Review Letters*, 107, 171103
- Zhu Y., Davis S. W., Narayan R., Kulkarni A. K., Penna R. F., McClintock J. E., 2012, *MNRAS*, in press, e-print arXiv:1202.1530